International Atomic Energy Agency Technical Meeting
Primary Radiation Damage: from nuclear reaction to point defects
1 - 4 October 2012
IAEA Headquarters, Vienna, Austria

Primary damage characteristics in metals under irradiation in the cores of thermal and fast reactors

V.A. Pechenkin et. al.

SSC RF Institute of Physics & Power Engineering, Obninsk, Russia

Outline

- Primary damage characteristics in different reactor irradiation environments
- Methods of experimental validation
- IPPE activities in the fields related

Introduction

- For an analysis and forecasting of radiation-induced phenomena in structural materials of WWERs, PWRs and BN reactors the fast neutron fluence is usually used

  for structural materials of the reactor core and internals the fluence of neutrons with energy >0.1 MeV,

  for WWER vessel steels the fluence of neutrons with energy >0.5 MeV in Russia and East Europe, and with energy >1.0 MeV in USA and France

- Displacements per atom (dpa) seem to be a more appropriate correlation parameter, especially, for structural materials of thermal reactors. The use of dpa allows to compare results of irradiation of materials in different neutron energy spectra or with different types of particles (neutrons, ions, fast electrons)

- Calculations of energy spectra of primary knocked atoms (PKA) and “effective” dpa, which are introduced to take into account the point defect recombination during the relaxation stage of a displacement cascade, are of both scientific and practical interests

Dose rate

At an arbitrary location in the material the dose rate *K* (dpa/s) is given by the following expression :

$$K = \int_{E_{min}}^{E_{max}} \sigma_d(E)\varphi(E)\, dE \qquad (1)$$

where $\varphi(E)$ is the incoming particles energy dependent flux, and $\sigma_d(E)$ is the displacement cross section

$$\sigma_d(E) = \int_{T_d}^{T_{max}} \frac{d\sigma\ (E,T)}{dT}\ \nu(T)dT \qquad (2)$$

where $\nu(T)$ is the number of displaced atoms per PKA of the energy T, $d\sigma(E,T)/dT$ is the differential cross section for the transfer of energy T to the struck atom from the incoming particle of energy E

Main errors in the dose rate calculations are introduced by T_d and $\nu(T)$

Displacement energy

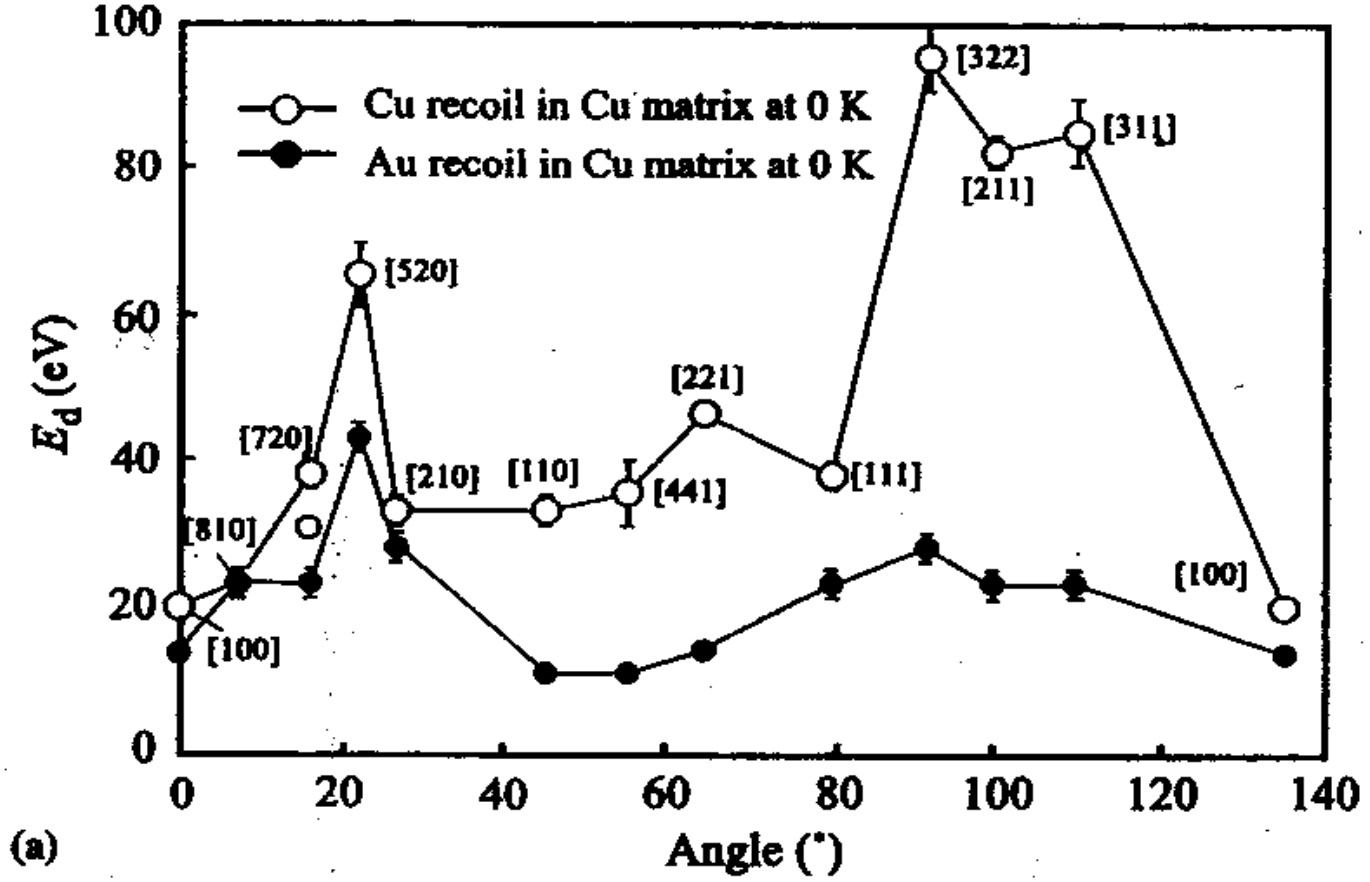

Displacement energy E_d as a function of recoil direction in (a) fcc Cu and Au crystal (after Bacon, 1993, from Was, 2007)

A lattice atom must receive a minimum amount of energy E_d in the collision to be displaced from its lattice site. Some averaged effective energy for each metal is used usually in displacement calculations.

Effective displacement energies

Metal	Lattice (c/a)	$E_{d,min}$ (eV)	E_d (eV)
Al	fcc	16	25
Ti	hcp (1.59)	19	30
V	bcc	–	40
Cr	bcc	28	40
Mn	bcc	–	40
Fe	bcc	20	40
Co	fcc	22	40
Ni	fcc	23	40
Cu	fcc	19	30
Zr	hcp	21	40
Nb	bcc	36	60
Mo	bcc	33	60
Ta	bcc	34	90
W	bcc	40	90
Pb	fcc	14	25
Stainless steel	fcc		40

Recommended values of the effective displacement energies for use in displacement calculations (from ASTM E521 (1996) Standard Practice)

Energy loss contributions

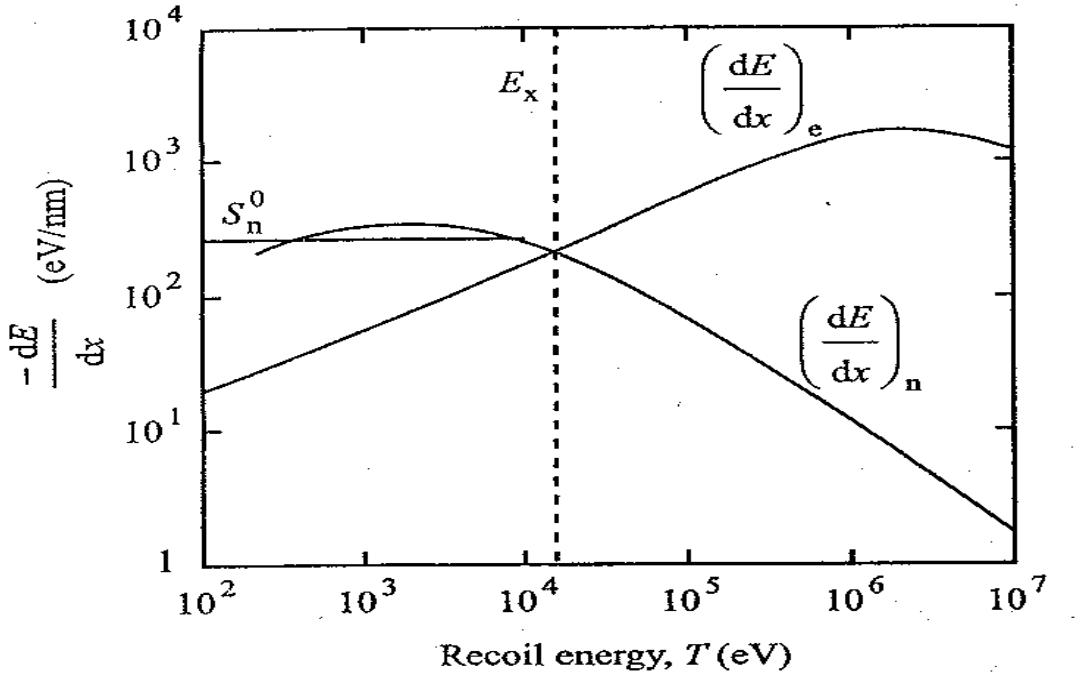

When an ion or atom (e.g. PKA) is traveling through a lattice, the total energy loss per unit length – dE/dx can be approximated by a sum of the components:

$$\left(-\frac{dE}{dx}\right)_{total} = \left(-\frac{dE}{dx}\right)_n + \left(-\frac{dE}{dx}\right)_e + \left(-\frac{dE}{dx}\right)_r, \qquad (3)$$

Where the subscripts are defined as follows:

n = elastic, e = electronic, r = radiation

For most of the applications energy loss by radiation is small.

In the simple Kinchin-Pease (1955) displacement model (hard-sphere elastic collisions) only elastic energy losses are accounted at $T<E_x$ and only electronic ones at $T>E_x$ for PKA

Damage effectiveness for various energetic particles

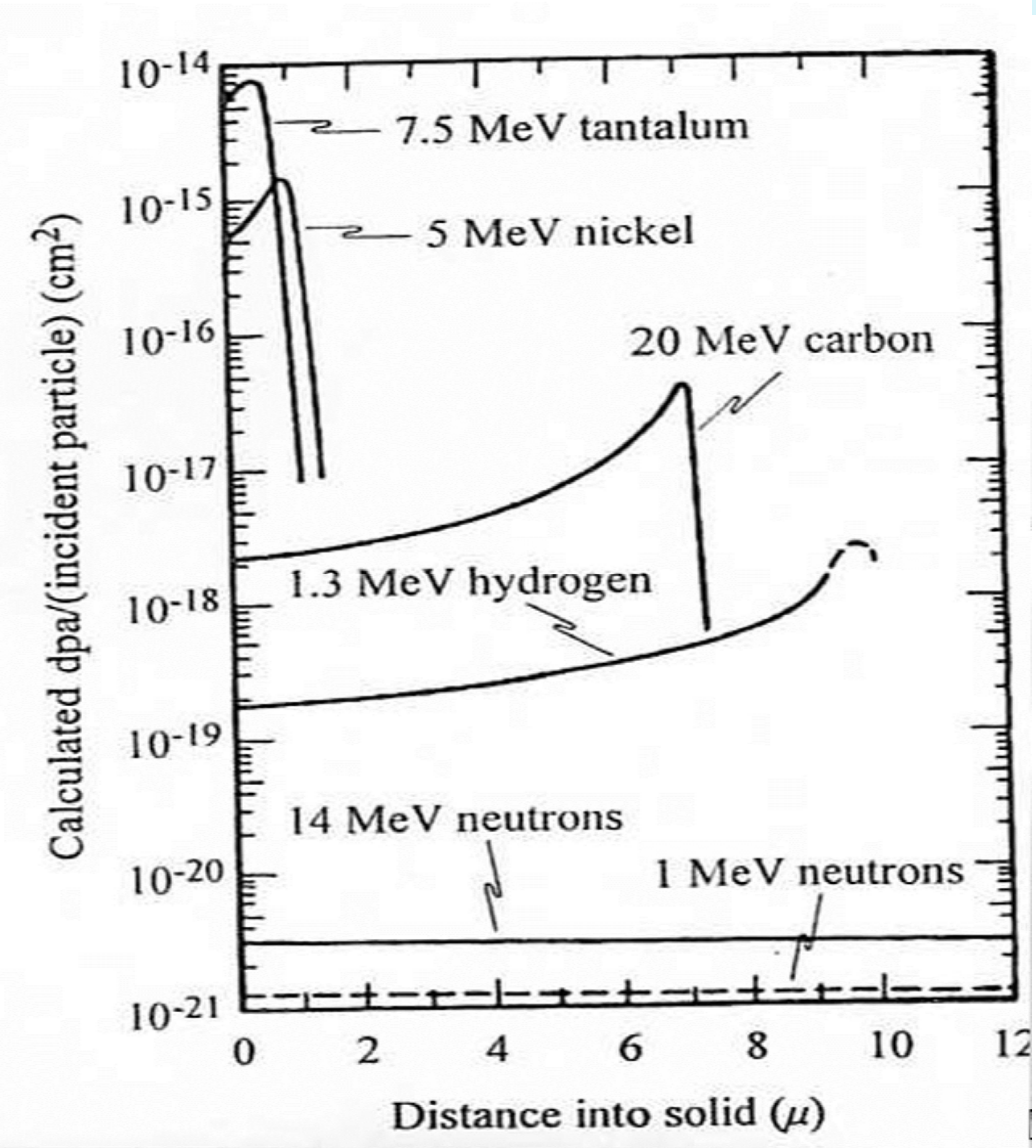

Displacement-damage effectiveness for various energetic particles in Ni (after Kulcinski, 1972)

Ions of heavier mass have a shorter penetration distance and higher damage rates

Displacement of atoms

Now the *NRT* – model (Norgett, Robinson and Torrens, 1975) is widely used for dpa calculations with Lindhard's partitioning between elastic and electronic energy losses:

$$\nu_{NRT} = \frac{0,8}{2T_d} T \frac{1}{1 + k_0 g(\varepsilon)} \qquad \textbf{(4)}$$

where $k_0 = 0,1337\ Z^{2/3} A^{-1/2}$; ($k_0 = 0,157$ **for Fe);**

$$g(\varepsilon) = \varepsilon + 0,4024\varepsilon^{3/4} + 3,401\varepsilon^{1/6} \quad ; \quad \varepsilon = T / 0,086937\ Z^{7/3}$$

($\varepsilon = T / 174,104$ **for Fe)**

***Z* – the atomic number, *A* – the atomic mass.**

Partitioning between elastic and electronic energy losses

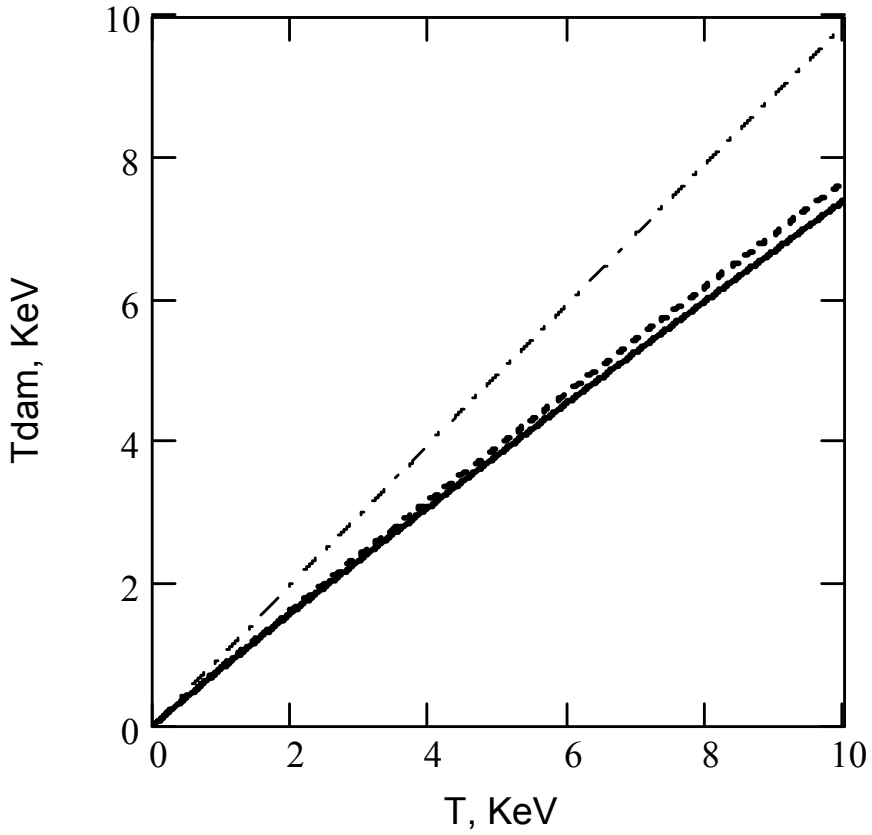

Fe – solid line

Zr - dashed line

Dashed-dotted line – linear approximation of the expression below

Here we denote

$$T_{dam} = \frac{T}{1 + k_0 g(\varepsilon)}$$

Stages of cascade development

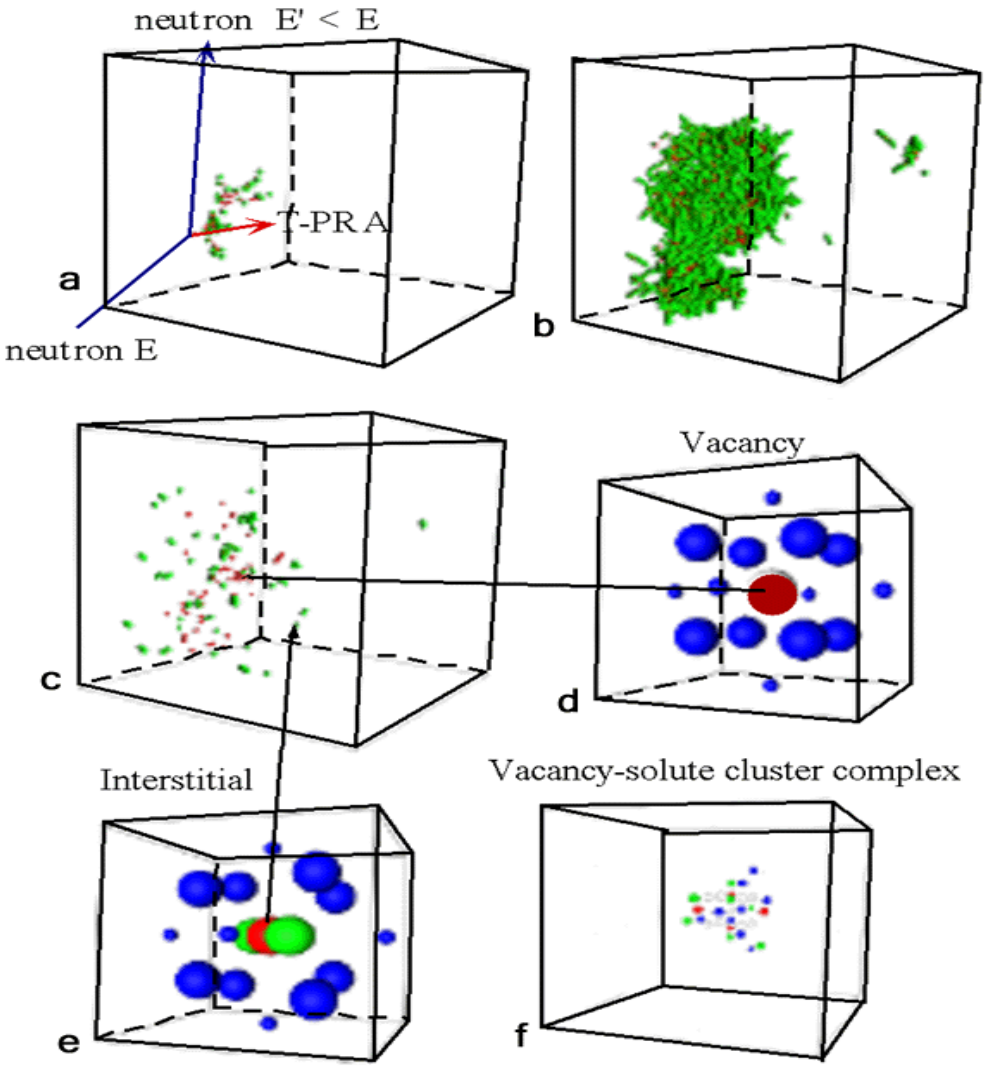

An illustration of cascade primary-damage production (iron atoms not shown in a–c and f): (a–c) MD simulation snapshots of initial, intermediate and final dynamic stage of a displacement cascade; (d–e) vacancy and self interstitial defects; (f) vacancy-solute cluster complex formed after long-term cascade aging (from Odette, 2001)

Stages of cascade development

Cascades evolve in stages and time-scale given as follows:

- *Collisional (< 0.1 ps).* A cascade of displacive collisions continues until no atom have enough energy to create further displacements

- *Thermal spike (~ 0.1 ps).* The spike occupies a region in which the energy is high enough so that the atoms resemble molten material

- *Quenching (~ 10 ps).* Molten zone returned to be condensed and thermodynamic equilibrium is established. The total number of point and clustered defects is much less than the number of atoms displaced in the collisional stage. “Effective” dpa after this stage

- *Annealing (> 1 ns).* This stage lasts until all mobile defects escape the cascade region. Additional correlated recombination

«Effective» dpa

Number of displacements per atom calculated with account of only defects surviving after in-cascade recombination will be called as «effective» dpa.

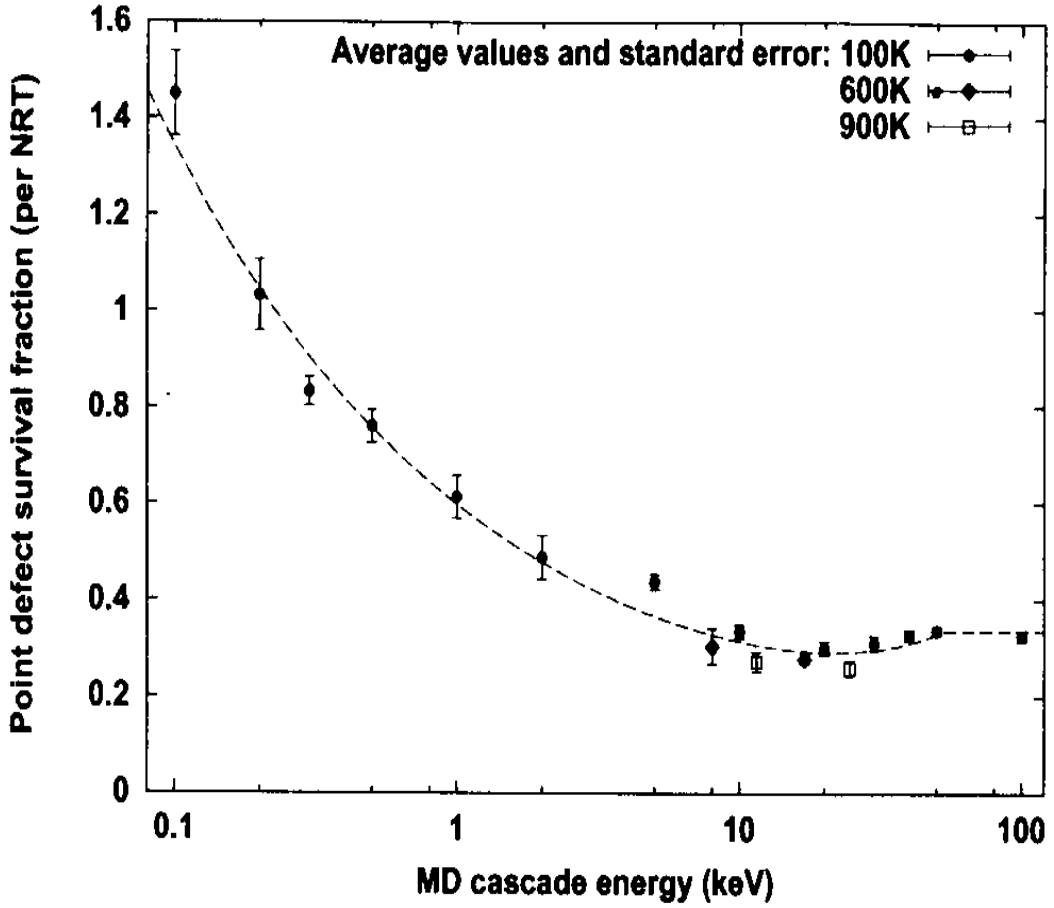

Energy dependence of total point defect survival η_{MD} in Fe obtained by R. Stoller, 2000, from MD cascade simulations. MD defect survival divided by NRT displacements.

The ratio $\eta_{MD}=\nu(T)/\nu_{NRT}(T)$ was approximated as follows:

$$\eta_{MD}=0.5608T^{-0.3029}+3.227\times 10^{-3}\ T$$

MD simulation uncertainties

- *Interatomic potentials used*
- *Account of electronic energy losses*

$$T_{MD} = \frac{T}{1 + k_0 g(\varepsilon)}$$

Cascade efficiency

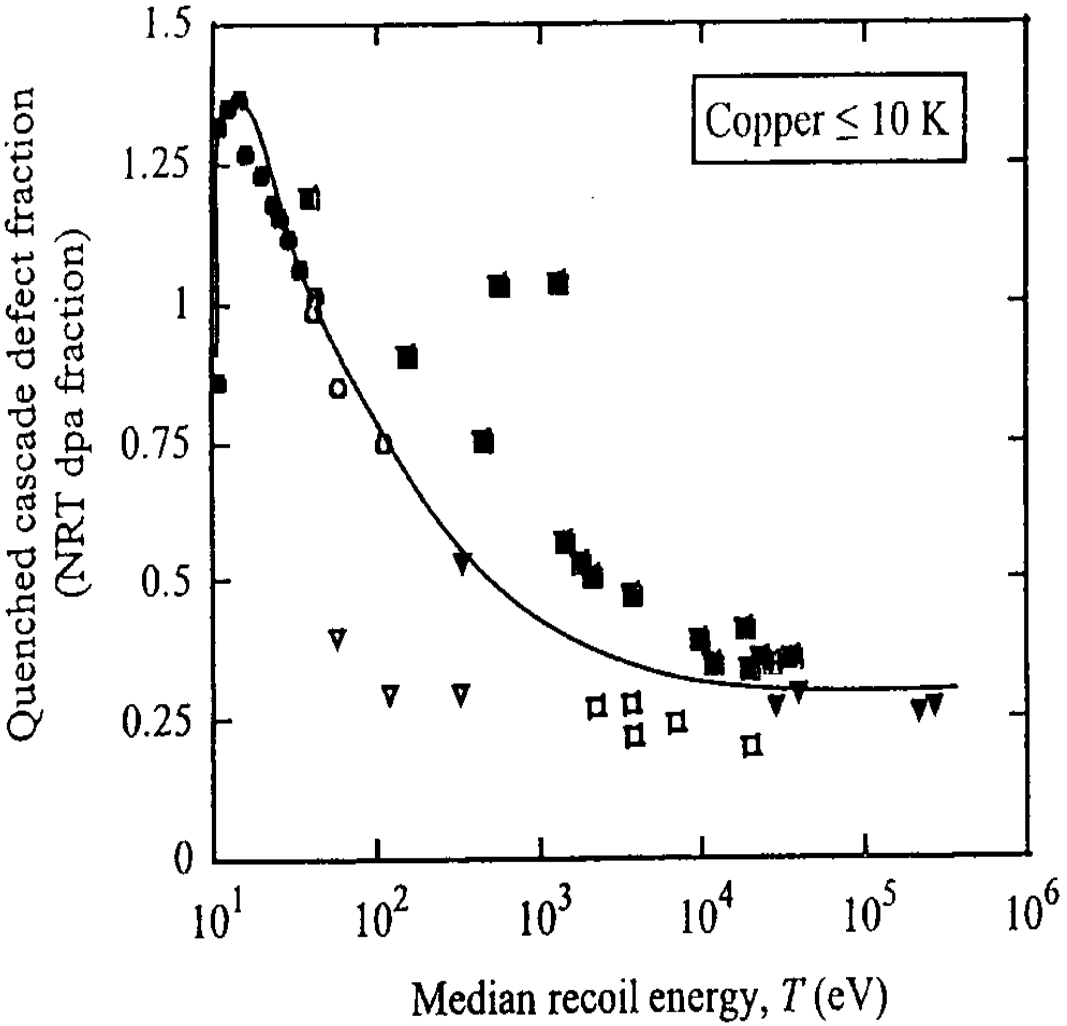

Dependence of the cascade efficiency $\eta=\nu(T)/\nu_{NRT}(T)$ on median PKA in copper.

Open symbols **refer to MD calculations and *filled symbols* refer to experimental measurements as the result of electron (●), ion (■), fission fragment (♦) and neutron (▼) irradiation at low temperatures**

(after Zinkle, 1993 , from Was, 2007)

Correlated recombination

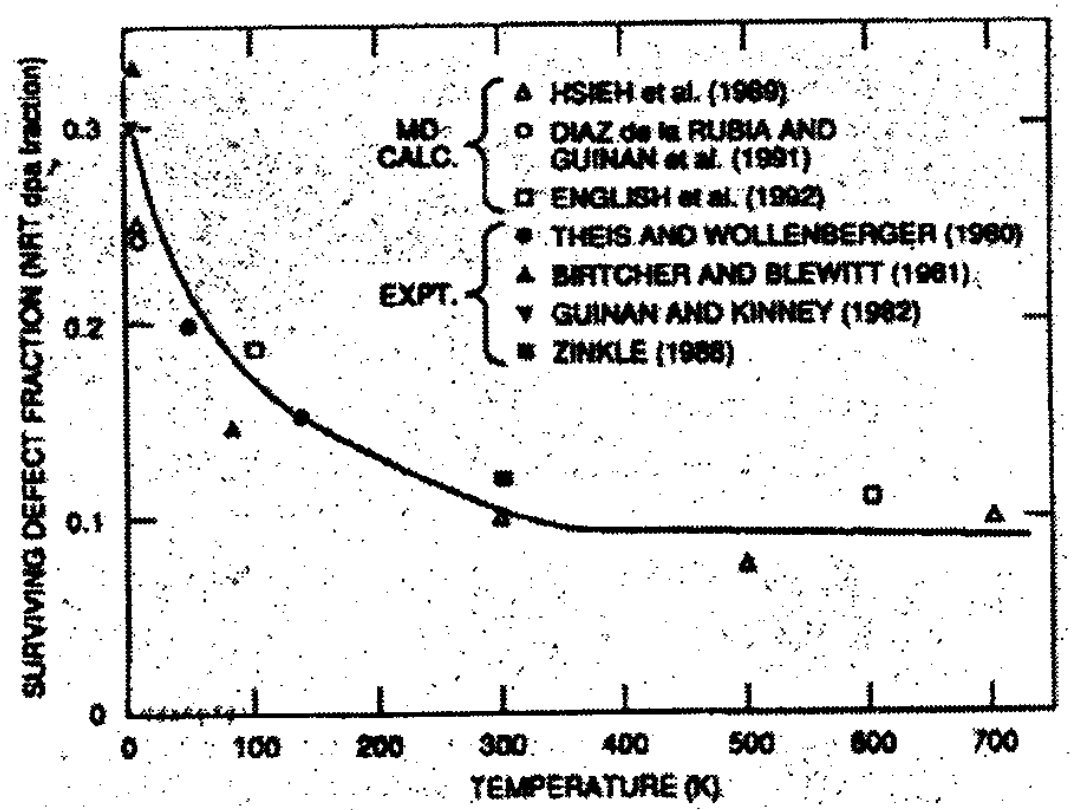

Fig. 4. Temperature-dependent fraction of defects surviving the cascade quench and correlated recombination (SDF) in copper irradiated under cascade conditions. The open symbols [20,43,74] refer to MD calculations performed with PKA energies of 3 to 5 keV and the filled symbols [52,53,72,73] refer to lower-bound estimates obtained from electrical resistivity measurements on neutron-irradiated copper (see text).

Zinkle, Singh, 1993
MD calculations and exp. data for **Cu**

At elevated temperatures a correlated recombination (CR) should be accounted for **VACs and SIAs (*electron irradiation*) and their moving clusters (*cascade conditions*). Acconting for CR, then surviving defect fraction:**

$$\eta_{CR} = \eta(1 - f_{CR})$$

Estimates by Theis, Wollenberger, 1980:

n and e irradiation of Cu

T = 90K; $f_{CR}^{n} = 0.65$; $f_{CR}^{e} = 0.55$

PKA – spectrum and «effective» dpa rate

Uncertainties in the neutron fluxes calculations in reactors and in the differential cross section data are much less then ones in estimates of T_d and $\nu(T)$

Changing the order of integration in the equation for the dose rate, one can find

$$K = \int_{T_d}^{T_{\max}} dT \cdot \nu(T) \cdot \int_{E_T}^{20\,MeV} \varphi(E) \cdot \frac{d\sigma\ (E,T)}{dT} dE \qquad (5)$$

where the integral over E is the spectrum of recoil energies (if $T>T_d$, then the spectrum of primary knocked atoms, PKA-spectrum)

The libraries of recoil energy spectra in *metals and alloys* can be created now for the irradiation facilities (in operation or shut down)

Substitution of $\nu_{NRT}(T)$ or $\nu_{MD}(T) = \eta(T)\ \nu_{NRT}(T)$ in (5) allows to calculate dpa (NRT) or "effective" dpa respectively

Primary damage characteristics in different reactor irradiation environments

Some damage characteristics : dpa (NRT), "effective" dpa, PKA-spectra are calculated in different locations of power reactors WWER-1000 and WWER-440 (both thermal reactors) and BN-600 and BR-10 (both fast reactors).

Besides, the radial function $K(r)$ that defines the ratio between the damage exposure in DPA units and in fast neutron fluence (FNF) units are calculated

$$K(r) = \int_{E_T}^{20MeV} \varphi(r,E)\sigma_{DPA}^{Fe}(E)dE \Big/ \int_{E_{fast}}^{20MeV} \varphi(r,E)dE$$

where $\sigma_{DPA}^{Fe}(E)$ is the DPA (NRT) cross-section for iron, E_{fast} is the lower energy boundary of the fast neutrons region (*0.1, 0.5 and 1.0 MeV*) and E_T is the lower energy boundary of the cross-section library used.

PKA energy spectrum in Fe and Zr in the core center of WWER-440

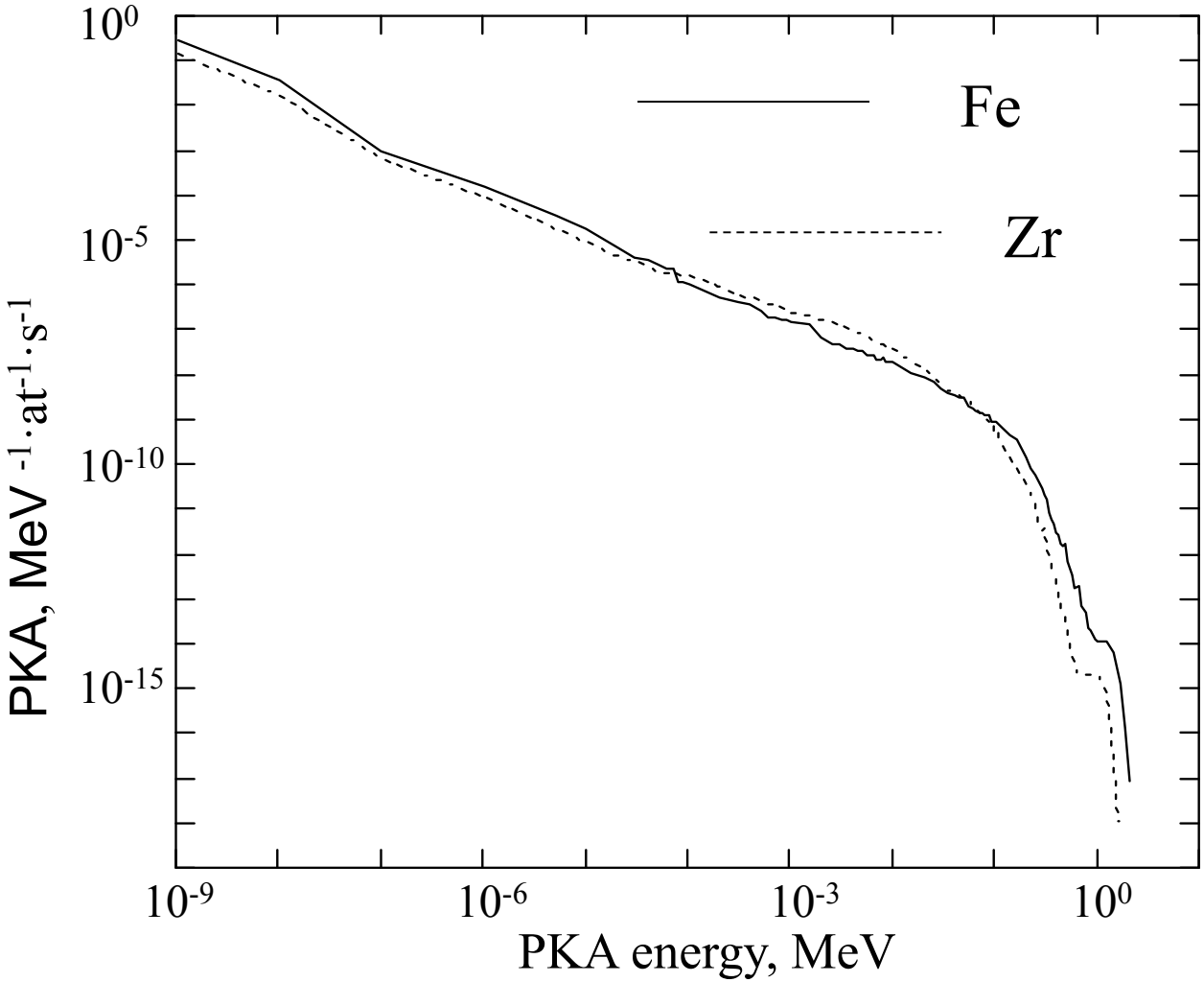

Generation rate of PKAs with the energies T from 40 eV (E_d for Fe and Zr) to 0.1 MeV is higher in Zr, but with higher T - in Fe

Neutron fluxes, dose rates and mean PKA energies in the core of WWER-440

Fast neutron flux, 10^{14} n/(cm^2×s)			Dose rate (effective dpa) 10^{-7} dpa/s		Mean energy of PKAs, keV	
E > 0.1 MeV	E > 0.5 MeV	E >1 MeV	Fe	Zr	Fe	Zr
1.77	1.26	0.853	1.24 (0.396)	1.32 (0.409)	15.6	8.89

Mean energy of PKAs is higher in Fe, but dose rates are similar in Fe and Zr

Relation between DPA and FNF units in WWER-1000

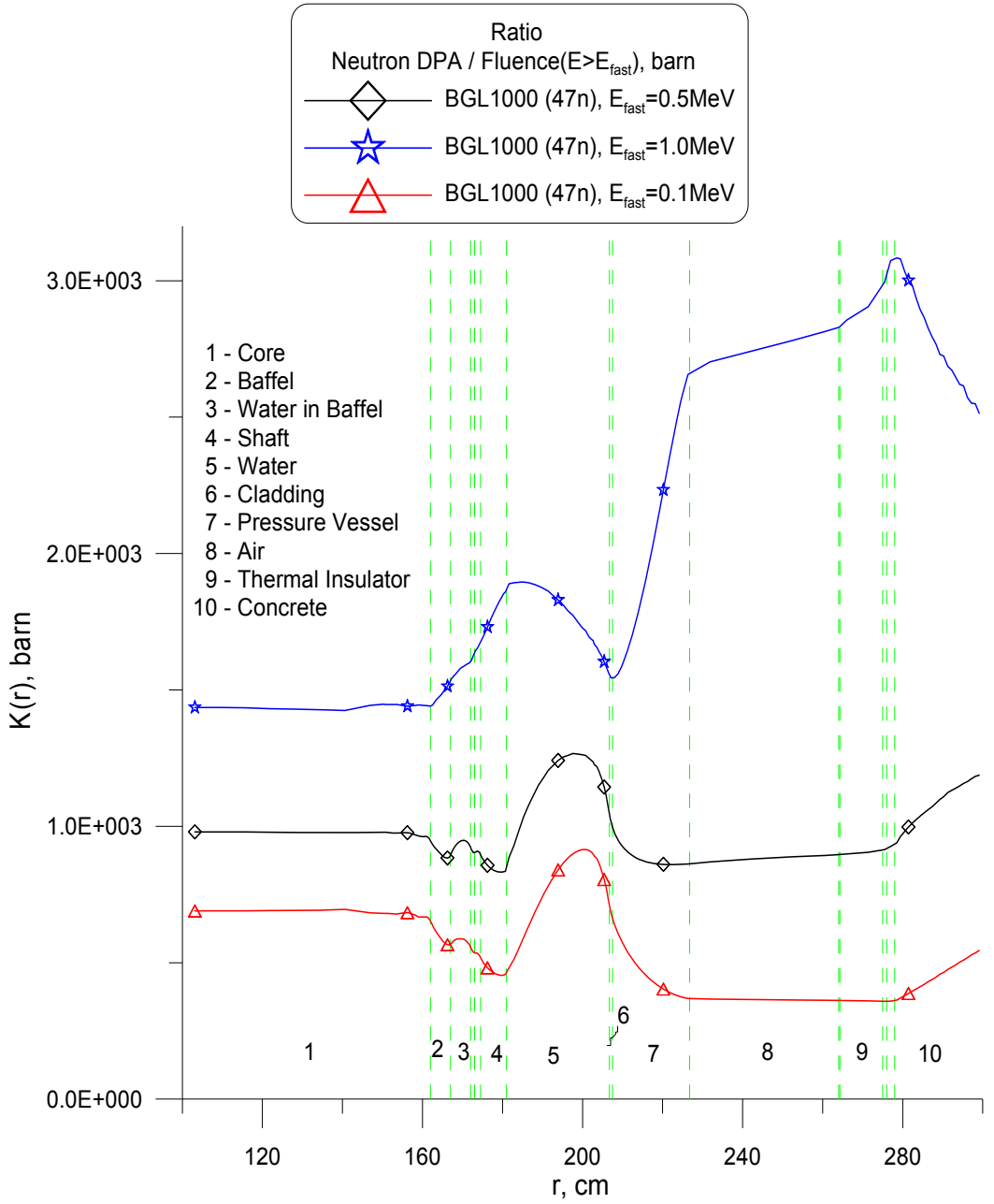

Ratio of the damage exposure in the DPA units to the one measured in the FNF units in the point $\vartheta = 10°$, $z = 211.8$ cm.

There is no linear dependence between damage exposure given in DPA and FNF units.

The FNF is not a universal quantity for definition of the damage exposure and the use of DPA for different elements of reactor construction seems more universal tool for this purpose, as it takes into account all available neutrons.

Neutron fluxes, dose rates and mean PKA energies in the core of reactors

Reactor	Material	Fast neutron flux, 10^{15} n/(cm^2×s) (dpa per fluence 10^{22} n/cm^2)		Dose rate, 10^{-7} dpa_{NRT}/s (dpa/year)	Dose rate, 10^{-7} dpa_{eff}/s (dpa/year)	Mean energy of PKA (keV)
		E>0.5 MeV	E>1 MeV			
WWER – 440	Fe	0.18	0.085	1.24	0.4	15.6
	Zr			1.32	0.41	8.89
WWER – 1000	Fe	0.21	0.1	1.47 (4.64)	0.47 (1.5)	15.9
	Zr			1.58 (5)	0.49 (1.54)	9.03
BN-600		3.70	0.79			
	Fe	(4.74)	(22.2)	17.6 (55.4)	5.92 (18.7)	7.23
	Zr	(5.51)	(25.9)	20.4 (64.5)	6.7 (21.0)	4.44
	Ti	(5.09)	(23.9)	18.9 (59.5)	8.9 (28.0)	3.70
	W	(1.21)	(5.66)	4.5 (14.1)	2 (6.21)	2.47

Contrary to expectations, the mean PKA energy in Fe in the cores of the thermal reactors is twice of that in the fast reactor

Dose rate in BN-600

Metal	R, cm	Dose rate, 10^{-8} dpa/s (dpa/year)					$\bar{T}$ Mean energy of PKA (keV)
		σ_{dpa}, standard spectrum	SPECTER				
			ν_{NRT} T_d = 40 eV (T_d^W = 90 eV)	ν_{NRT} T_d = 30 eV (T_d^W = 90 eV)	SPECTER	ν_{MD}	
Fe	19.8	172 (54.2)	176 (55.4)	234 (73.8)	172 (54.3)	59.2 (18.7)	7.23
	69.3	161 (50.7	164 (51.8)	219 (69.0)	161 (50.8)	54.9 (17.3)	7.89
	89.1	136 (42.9)	139 (43.7)	185 (58.3)	136 (42.9)	46.1 (14.5)	8.40
	108.9	48.4 (15.3)	49.5 (15.6)	66.0 (20.8)	48.6 (15.3)	17.3 (5.44)	5.33
	128.7	5.09 (1.61)	5.24 (1.65)	6.98 (2.20)	5.15 (1.62)	1.97 (0.622)	3.02
Ti	19.8	222 (69.9)	189 (59.5)	251 (79.4)	192 (60.5)	88.7 (28.0)	3.70
	69.3	203 (64.0)	174 (55.0)	232 (73.3)	177 (55.8)	81.0 (25.5)	4.18
	89.1	169 (53.4)	146 (46.2)	195 (61.5)	149 (46.9)	67.6 (21.3)	4.55
	108.9	67.6 (21.3)	55.7 (17.6)	74.3 (23.4)	56.6 (17.9)	27.2 (8.58)	2.55
	128.7	8.51 (2.68)	6.70 (2.11)	8.93 (2.82)	6.81 (2.15)	3.53 (1.11)	1.45
Zr	19.8	198 (62.6)	204 (64.5)	273 (86.0)	205 (64.7)	66.6 (21.0)	4.44
	69.3	185 (58.4)	191 (60.1)	254 (80.2)	191 (60.3)	61.7 (19.5)	4.74
	89.1	156 (49.2)	160 (50.6)	214 (67.4)	161 (50.8)	51.7 (16.3)	4.97
	108.9	56.2 (17.7)	58.3 (18.4)	77.8 (24.5)	58.6 (18.5)	19.4 (6.12)	3.51
	128.7	5.98 (1.89)	6.29 (1.98)	8.39 (2.65)	6.33 (1.99)	2.20 (0.693)	2.32
W	19.8	46.7 (14.7)	44.9 (14.1)	44.9 (14.1)	50.3 (15.9)	19.7 (6.21)	2.47
	69.3	43.7 (13.8)	42.1 (13.3)	42.1 (13.3)	47.5 (15.0)	18.1 (5.71)	2.64
	89.1	37.0 (11.7)	35.7 (11.3)	35.7 (11.3)	40.5 (12.8)	15.1 (4.76)	2.76
	108.9	13.0 (4.11)	12.4 (3.90)	12.4 (3.90)	13.6 (4.30)	5.89 (1.86)	1.95
	128.7	1.36 (0.428)	1.25 (0.394)	1.25 (0.394)	1.31 (0.414)	0.700 (0.221)	1.28

Neutron fluxes, dose rates and mean PKA energies in the core of experimental fast reactor BR-10

Material	Neutron flux, 10^{15} n/(cm^2×s) (dpa per fluence 10^{22} n/cm^2)		Dose rate 10^{-7} dpa/s (dpa/year)		Mean energy of PKA, keV
	E>0.1 MeV	E>1 MeV	ν_{NRT}	ν_{MD}	
Fe	0.95 (5.73)	0.36 (15.0)	5.4 (17.1)	1.74 (5.50)	17.2

This reactor is shut down now, but many experimental data were obtained and published during its operation

Recoil energy spectra

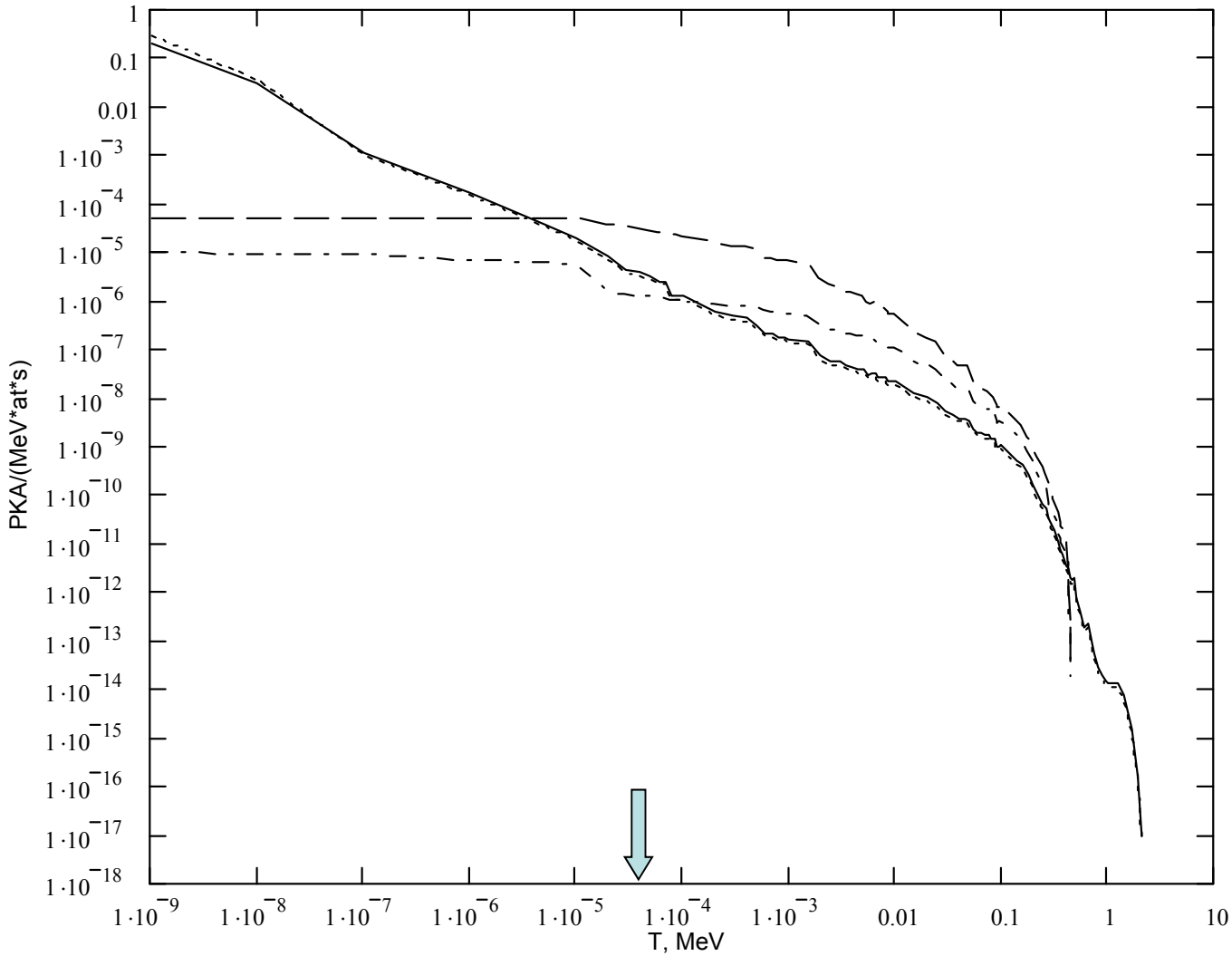

Recoil energy spectra in Fe in the cores of BN-600 (dashed line, T_m = 7.23 KeV), VVER-440 (dotted line, T_m = 15.6 KeV), and VVER-1000 (solid line, T_m = 15.9 KeV) and BR-10 (dashed-dotted line, T_m = 17.2 KeV)

Methods of experimental validation

Nondirect methods

- Mechanical properties at low temperatures
- Resistivity measurements at low temperatures
- Radiation-enhanced (or –induced) grows of the Ni3Si layer on the surface of Ni-S- alloy at elevated temperatures

- Radiation-induced segregation (?) at elevated temperatures

Yield strength

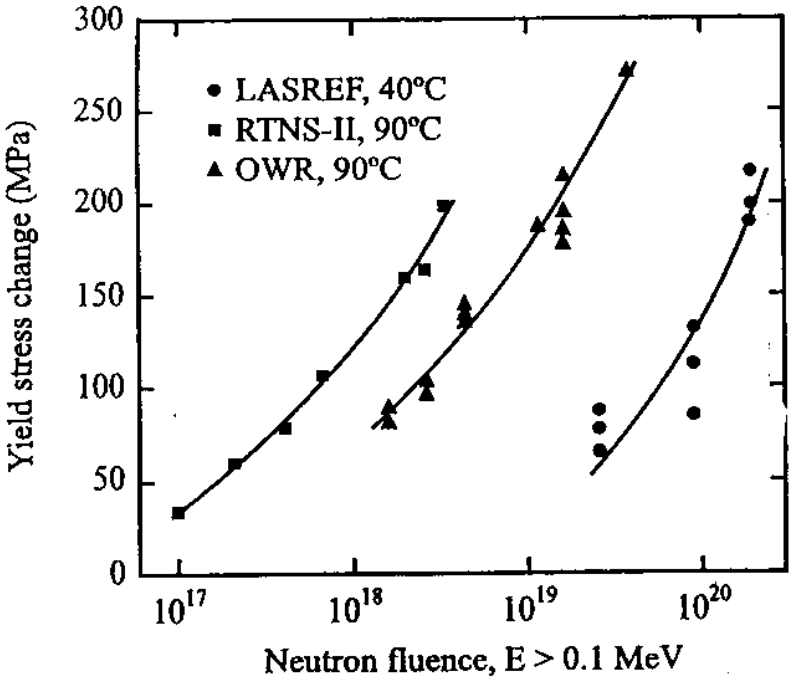

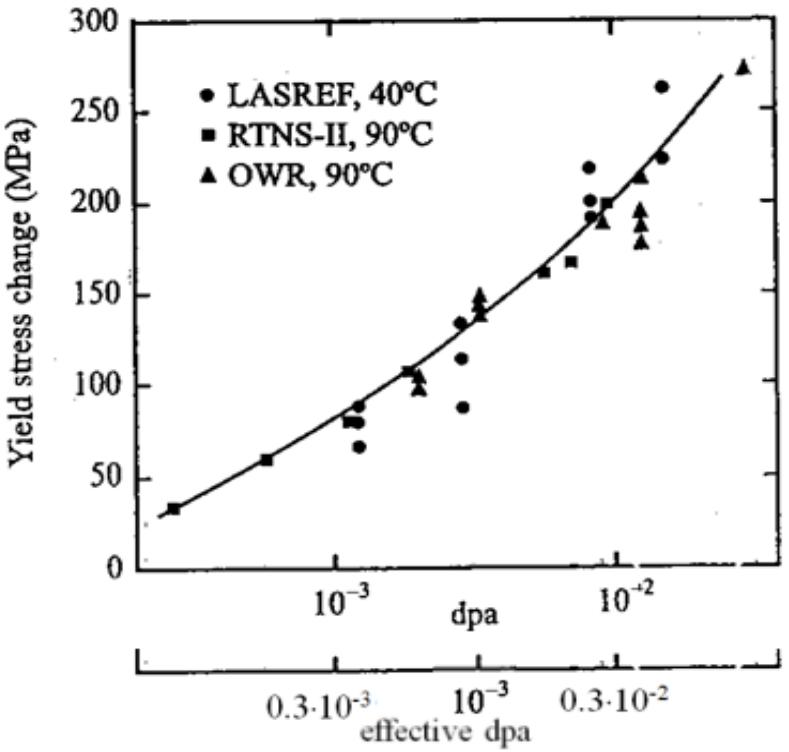

The increases in yield strength arising in single heat of 316 stainless steel during irradiation at relatively low temperatures in very diverse neutron spectra. OWR was a test reactor that had a typical LWR spectrum; RTNS-II produced a pure 14 MeV source and LASREF a very broad spectrum of high neutron energies (after Grenwood, 1994, from Was, 2007)

While there is little correlation in terms of neutron fluence, the yield stress changes correlate well against damage dose in displacements per atom, dpa

Electrical resistivity measurment

Broeders and Konobeev, 2004: damage resistivity rate in metals and in 300 series SS at low temperature irradiation in different neutron spectra agrees with “effective” dpa

There are large differences in the data on resistivity per FP (RFP)

Difference in RFP between electron and neutron irradiations should be accounted for (effect of clustering)

Radiation-enhanced (or –induced) grows of the Ni_3Si layer

In a number of earlier papers a very low cascade efficiency in the production of freely migrating defects (η_{FMD}) was estimated under ion irradiation by fitting the Ni_3Si layer growth on the surface of Ni-Si alloy to the simple model (Rehn et al., 1984, 1987, и др.).

Cascade efficiency in FMD production

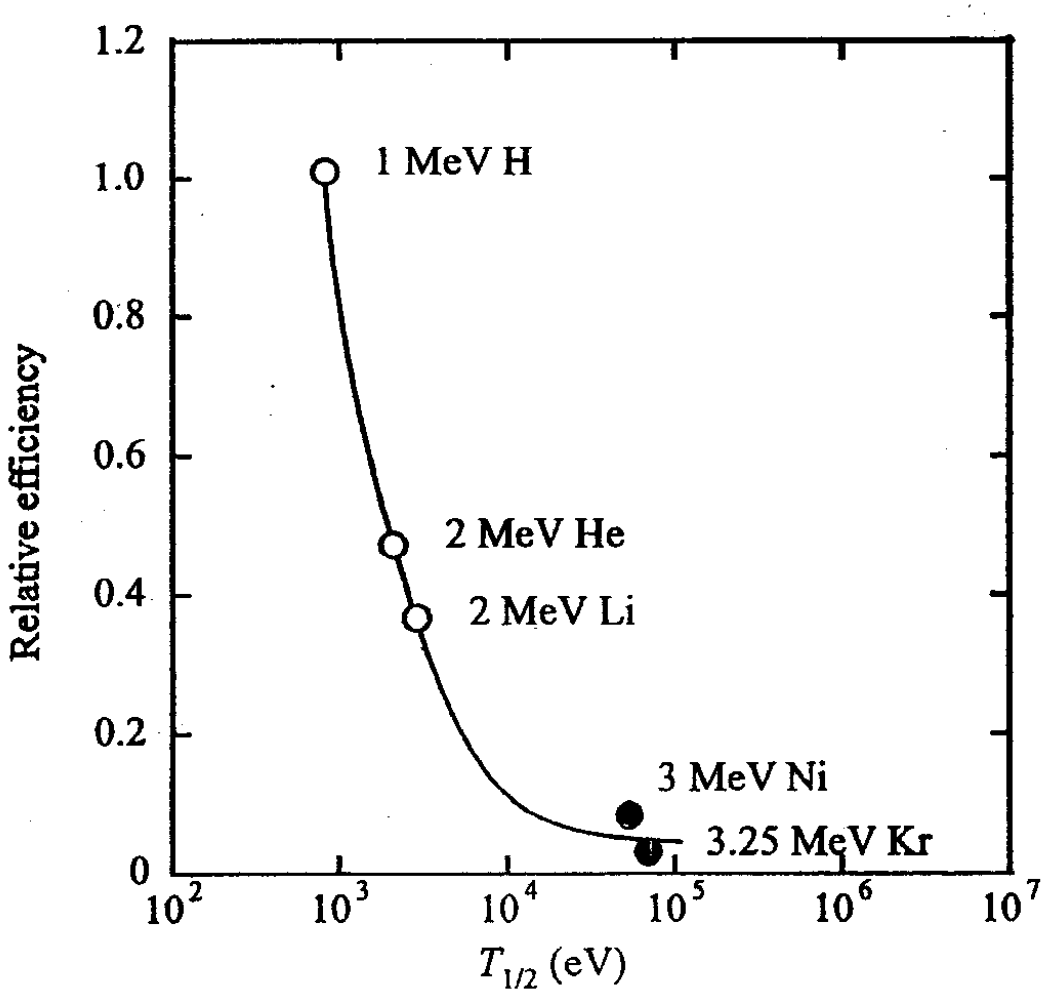

Fig. 3.19. Relative efficiency of freely migrating defect production for ions of various mass and energy (after [20])

Estimates of low cascade efficiency in the production of freely migrating defects (Ni_3Si layer grows) on the base of early model predictions

From Rehn, 1984

Cascade efficiency in FMD production

However in more resent papers (Rehn and Wiedersich, 1992; Iwase, Rehn 1996 и др.) it was shown that earlier values of a very low cascade efficiency η_{FMD} are obtained not due to strong intracascade recombination but due to the effect of very high sink strength for moving PD supplying the growing layer with Si

Radiation-induced segregation
Ion irradiation

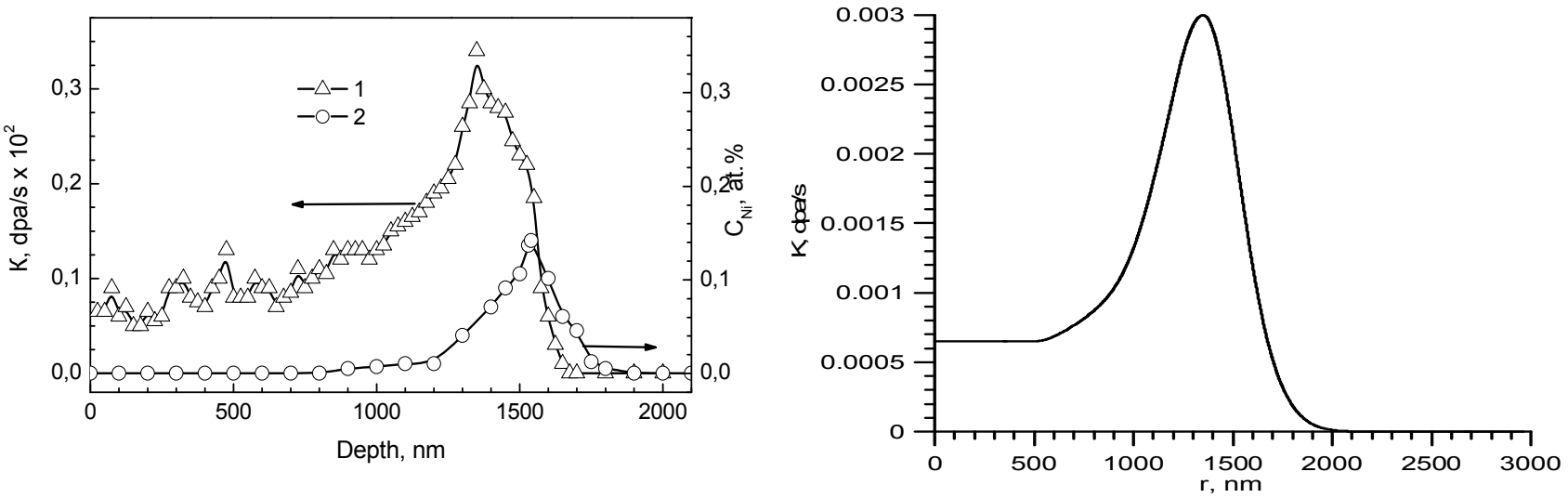

Depth profiles of damage rate and implanted ions in EP-823 steel (TRIM-98 code) after irradiation with 7 MeV Ni^{++} ions in the ion accelerator EGP-15 (IPPE): 1 – dose rate K; 2 – C_{Ni} (dose = 10 dpa); on the right – damage rate profile approximation used in calculations for 7 MeV nickel ions

Radiation-induced segregation

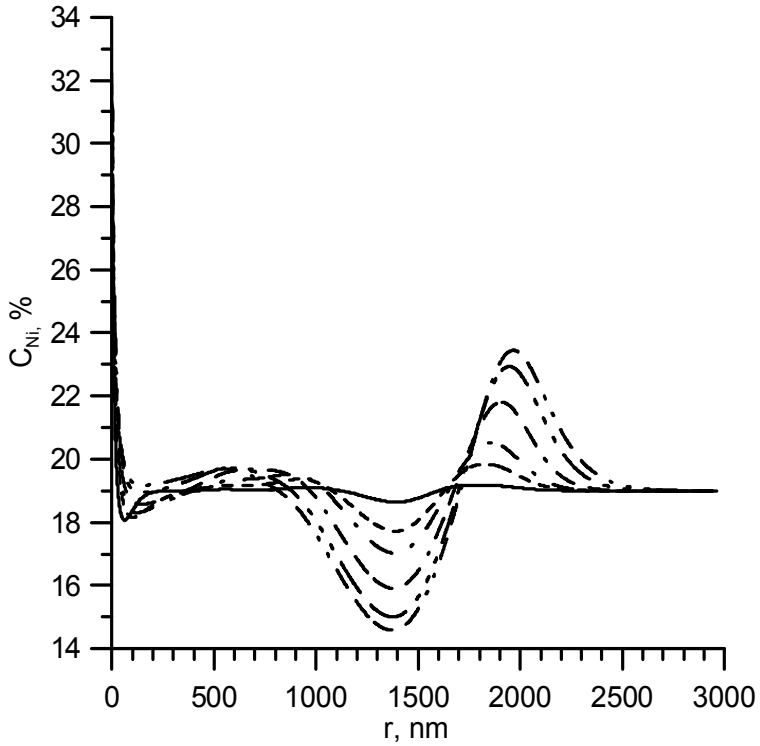

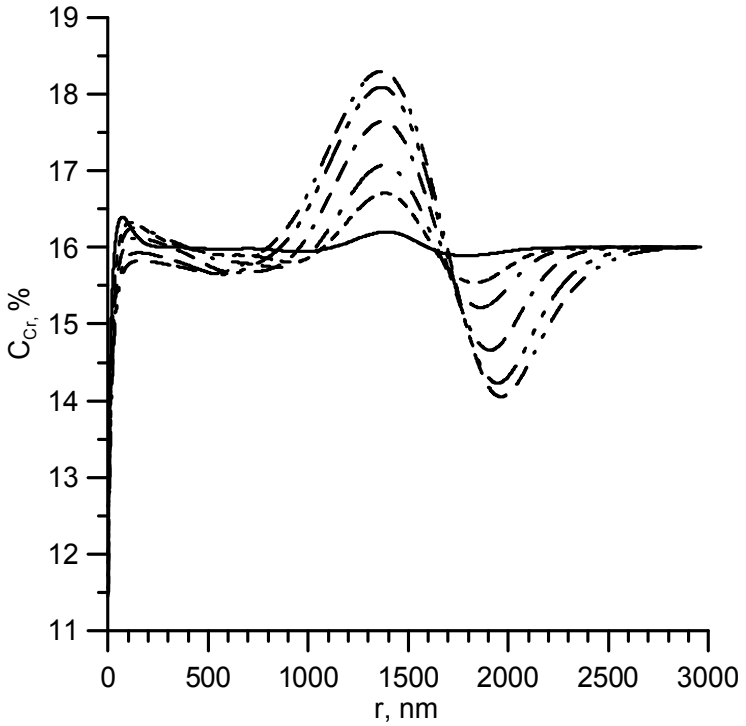

Component profiles along the projected range in Fe–19Ni–16Cr alloy under irradiation with Ni^{++} ions at different times:

—— *1000 s (0.65 dpa* near the surface*),* ------ *5000 s (3.25 dpa),* – · – · *10000 s (6.5 dpa),*

– – · *25 000 s (16.25 dpa),* — · · · *50 000 s (32.5 dpa),* – – · · *70 000 s (45.5 dpa)*

Radiation-induced segregation

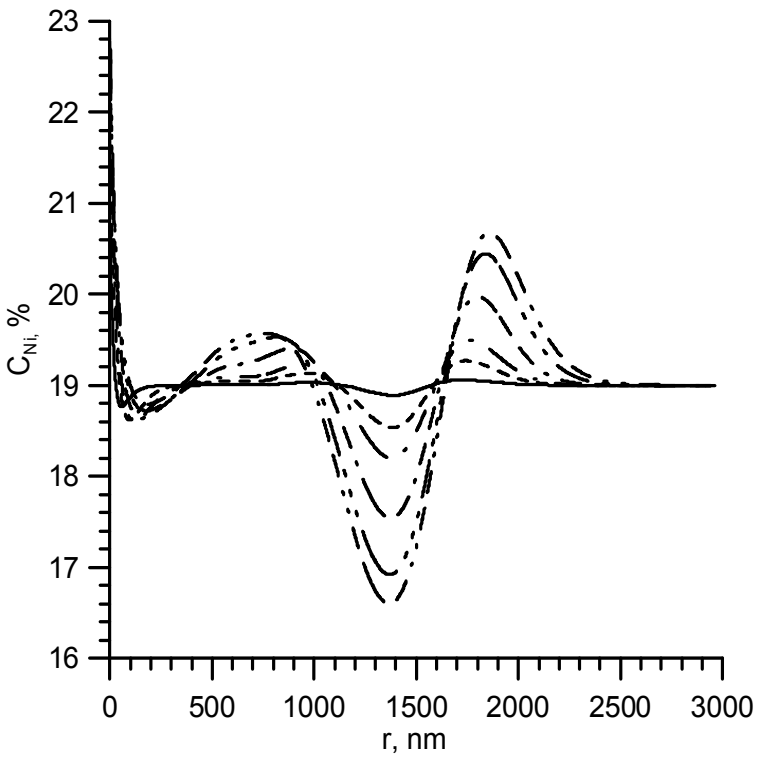

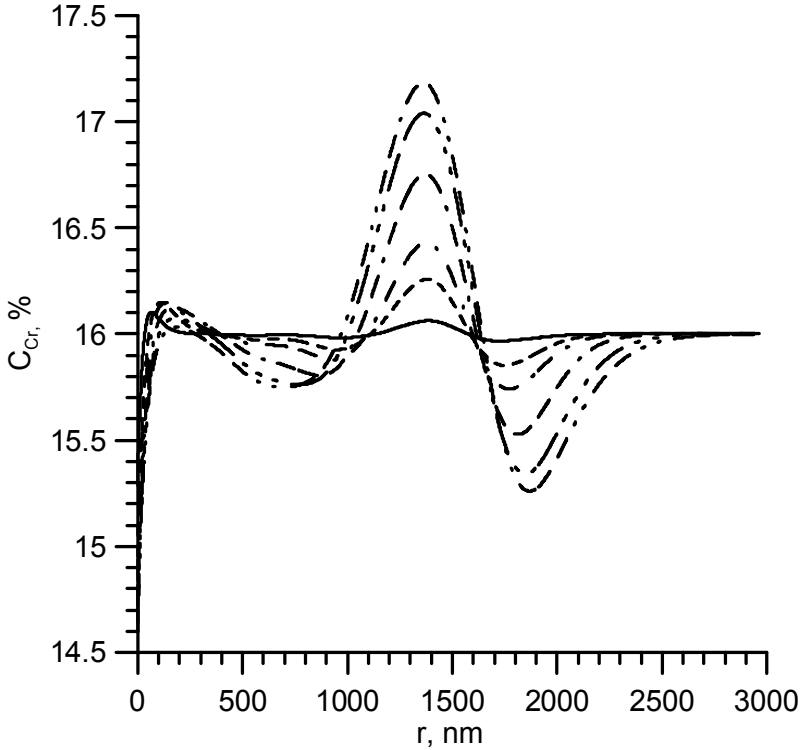

Component profiles along the projected range in Fe–19Ni–16Cr alloy under irradiation with Ni^{++} ions at different times with PD generation rates divided by ten: ——— *1000 s,* - - - - - - *5000 s,* – · – · *10000 s,* – – · *25000 s,* — · · · *50 000 s,* – – · · *70 000 s*

Radiation-induced segregation

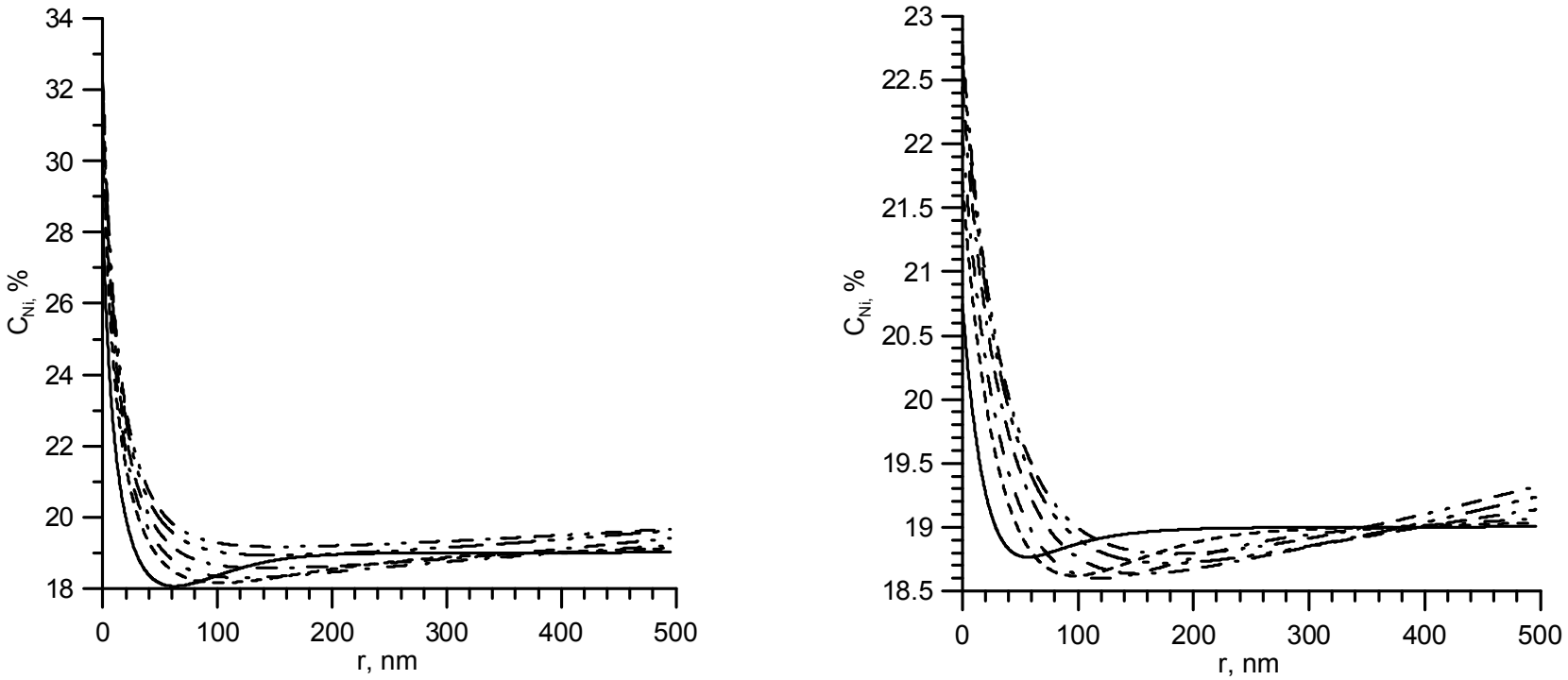

Ni profiles along the projected range in Fe–19Ni–16Cr alloy under irradiation with Ni^{++} ions at different times (on the right – with PD generation rates divided by ten):

——— *1000 s (0.65 dpa* near the surface*)*, - - - - - - *5000 s (3.25 dpa)*, – · – · *10000 s (6.5 dpa)*,

– – · *25 000 s (16.25 dpa)*, — · · · *50 000 s (32.5 dpa)*, – – · · *70 000 s (45.5 dpa)*

Radiation-induced segregation

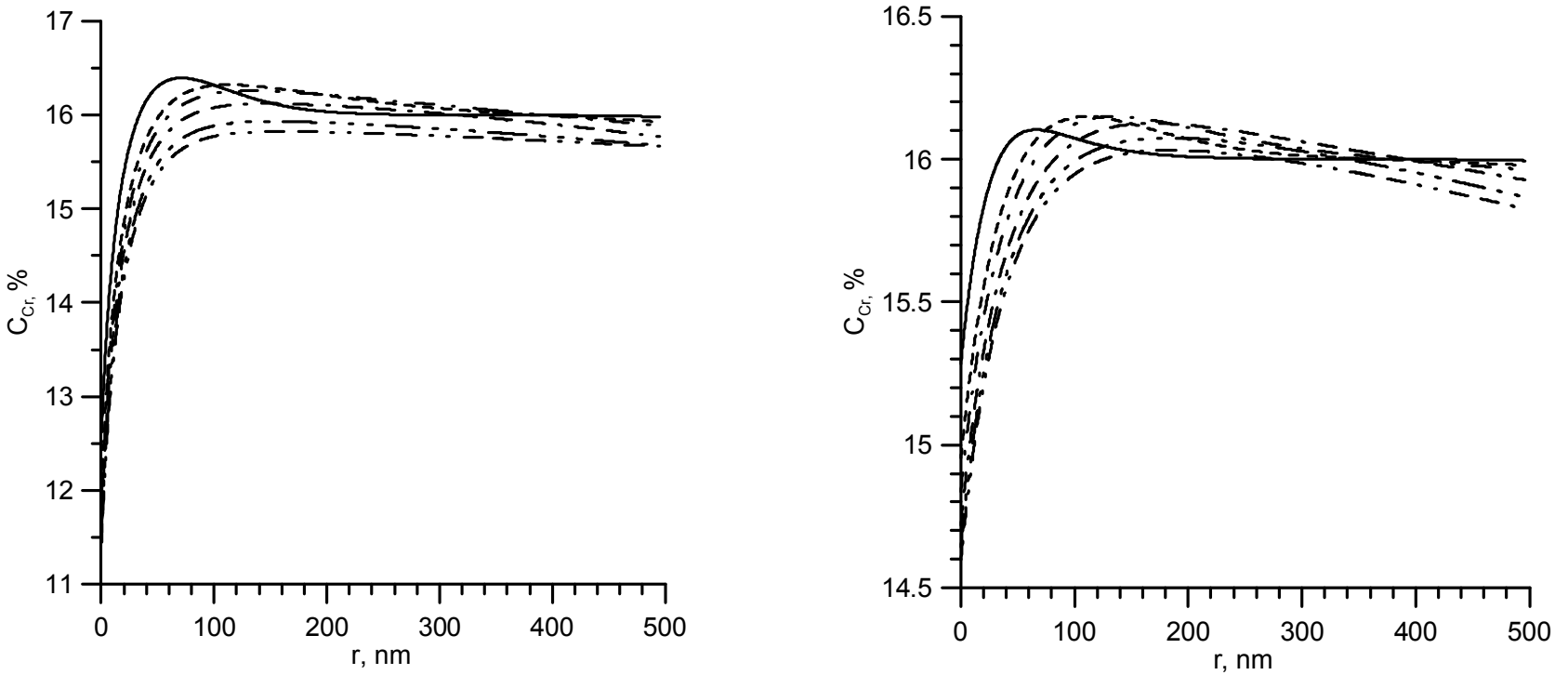

Cr profiles near the surface in Fe–19Ni–16Cr alloy under irradiation with Ni^{++} ions at different times (on the right – with PD generation rates divided by ten):
——— *1000 s,* ------ *5000 s,* –·–· *10 000 s,* – – · *25 000 s,*
—·–· *50 000 s,* – – ·· *70 000 s*

Radiation-induced segregation

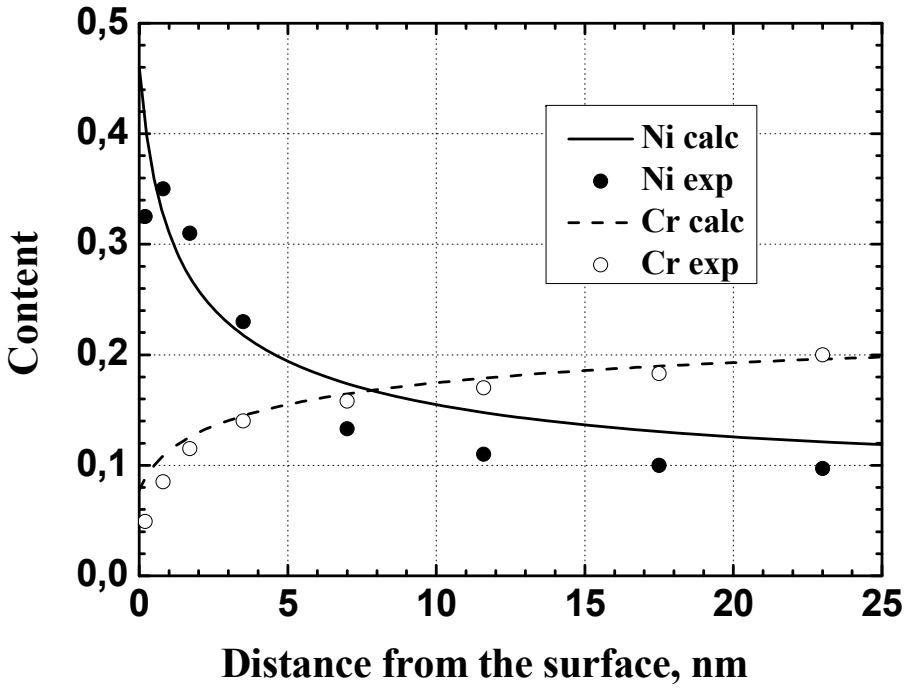

Results of RIS numerical calculations fitted to the data by Sethi and Okamoto (1981) on component segregation near a sample surface of Fe-20Cr-12Ni alloy irradiated with 3 MeV Ni ions to 6 dpa *at a damage rate of* 2×10^{-3} *dpa/s*

Results should be recalculated accounting for damage rate and cascade efficiency variations along the track

IPPE activities in the fields related

- Calculation of neutron fluxes and damage dose characteristics in metals and alloys under irradiation in the cores of Russian power reactors

WWER- 440,-1000

BN-600,-800,-1200, BREST

BR-10, BOR-60, MBIR

IPPE activities in the fields related

- Calculation of damage dose characteristics in metals along projected range under ion irradiation

7 MeV Ni^{++} ions in the ion accelerator EGP-15 (IPPE):

1.8 MeV Cr+3 ions typical for ESUVI accelerator at KIPT

Tandem electrostatic accelerator EGP-15 at IPPE

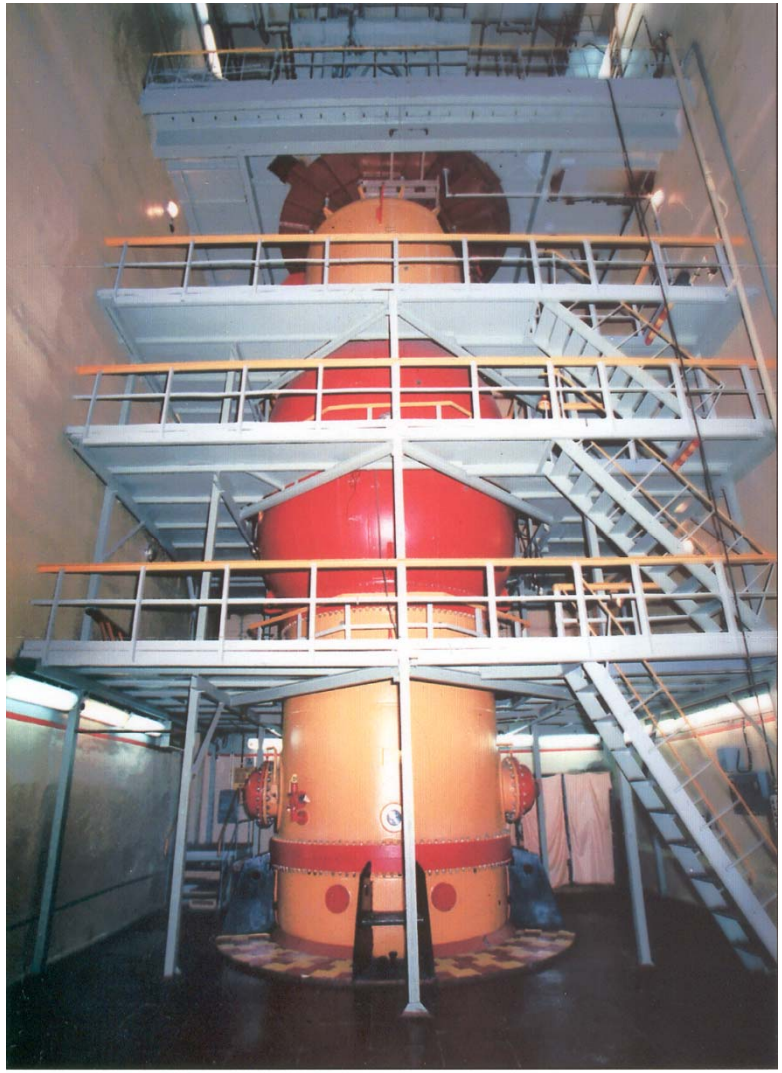

- Ion current: from several dozen nanoA up to hundreds microA
- Ion energy: from several dozen keV up to dozen MeV
- Ions: H, He, Li, B, C, N, O, F, Al, P, S, Cl, Fe, **Ni**, Cu, Zr and others

Point defect generation profiles in EP-823 steel under irradiation with various ions

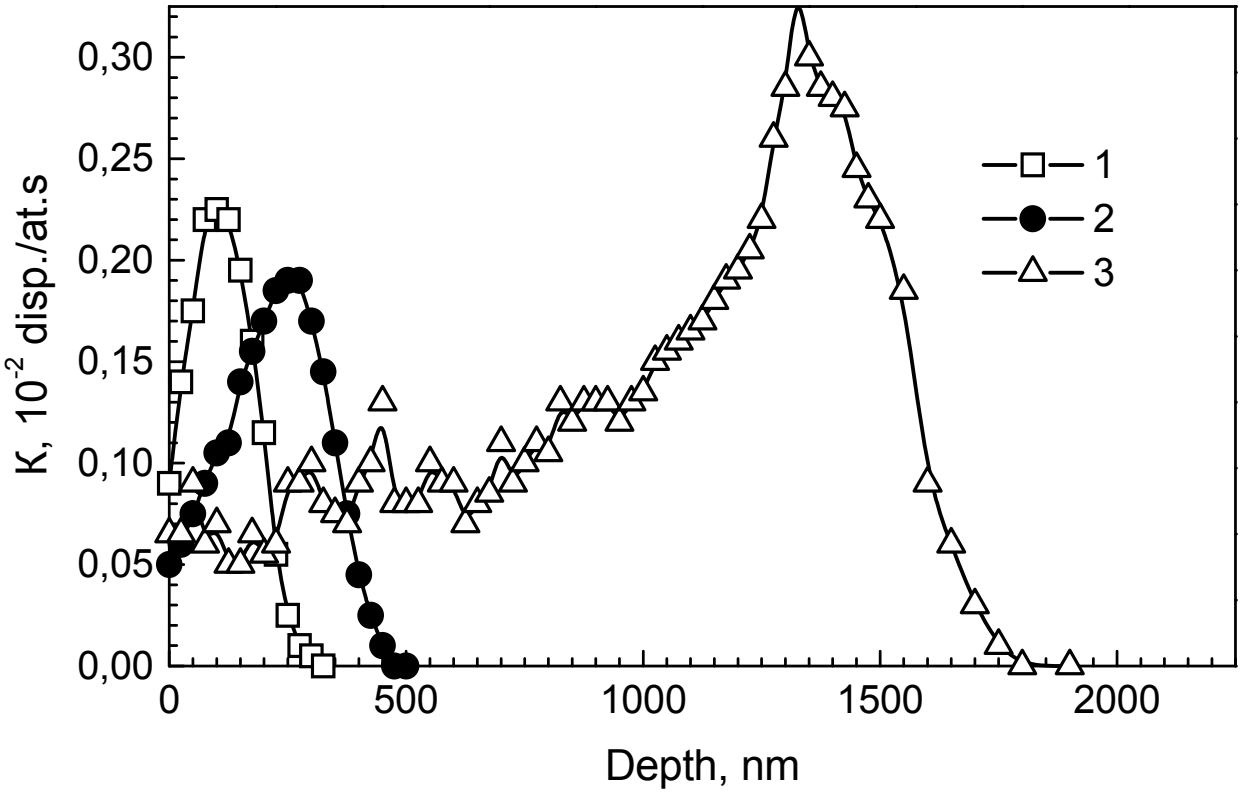

Displacement generation rates (dpa/s) profiles in EP-823 steel under irradiation with various ions calculated by using the TRIM-98 code : **1**-He^{+} ions, 30 keV; **2**- He^{+} ions, 70 keV (ILU-100 accelerator); **3**- Ni^{++} ions, 7 MeV

RIS in EP-823 steel irradiated with Ni^{++} and He^{+} ions

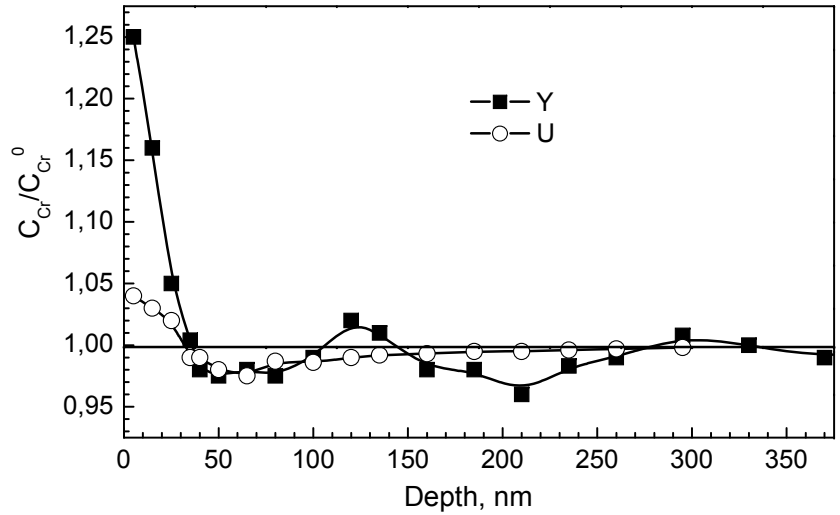

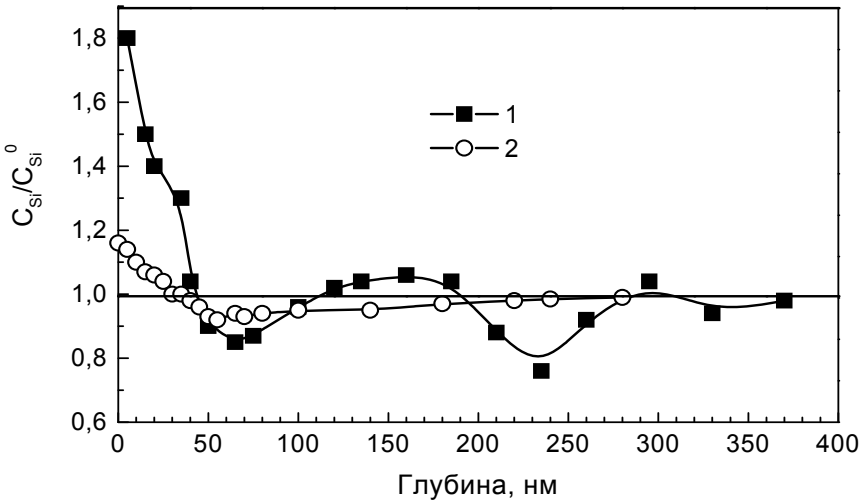

Ferritic-martensitic steel EP-823 was irradiated with 7 MeV Ni^{++} ions at **EGP -15** (penetration depth ~ 1400 nm) and also
with 70 keV He^{+} ions at **ILU -100** (penetration depth ~ 240 nm)
at the temperature of 500°C.

The depth distribution of Cr and Si measured by X-ray photoelectron spectroscopy

1 - He^{+}, 2×10^{20} ion/m^2 (0.2 dpa);
2 – Ni^{++}, 6×10^{18} ion/m^2 (0.2 dpa)

IPPE activities in the fields related

Radiation-induced segregation (RIS) leads to significant changes in alloy composition near main microstructural features: grain boundaries and sample surfaces, dislocations, precipitates, voids and strongly effects the precipitate phase composition, swelling, embrittlement and other radiation phenomena.

- Modeling of RIS in two-, three- and four-component substitution alloys near sample surface, grain boundaries and also near cylindrical (dislocations) and spherical (precipitates and voids) point defect sinks

IPPE activities in the fields related

- Gas production: estimation of (n, alpha) reaction cross section for chromium isotopes

The (n,α) reaction cross section of chromium isotopes has significant role in radiation resistance of stainless steel, which is wildly used in nuclear reactor industry. In EXFOR there is only limited number of experimental data for this reaction and mainly they take place at 14 MeV. The experimental data for (n,α) reaction probability in fission neutron energy range are almost absent. In this work results for 50Cr(n,α) and 52Cr(n,α) reaction excitation function investigations are presented

Chromium isotopes properties

Isotope	**Natural abundance, %**	**(n,α) reaction Q-value, MeV**
^{50}Cr, $T_{1/2}>1,8*10^{17}$ y, EC	4,345	+0,3213
^{52}Cr, stable	83,489	-1,2097
^{53}Cr, stable	9,501	+1,7903
^{54}Cr, stable	2,365	- 1,5466

Present status of experimental data and evaluation for chromium isotopes

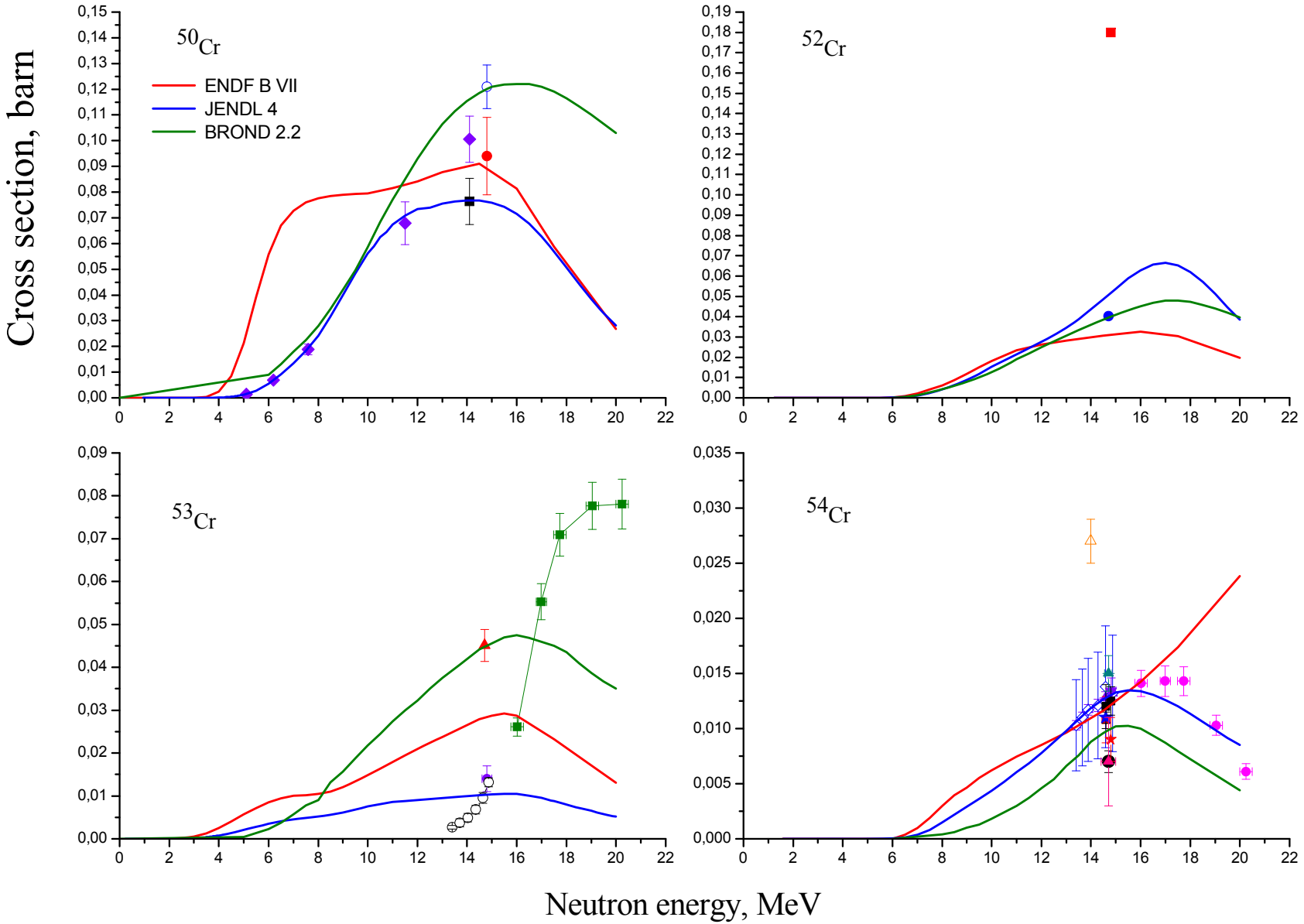

Status of theoretical evaluation for $^{50}Cr(n,\alpha)^{47}Ti$

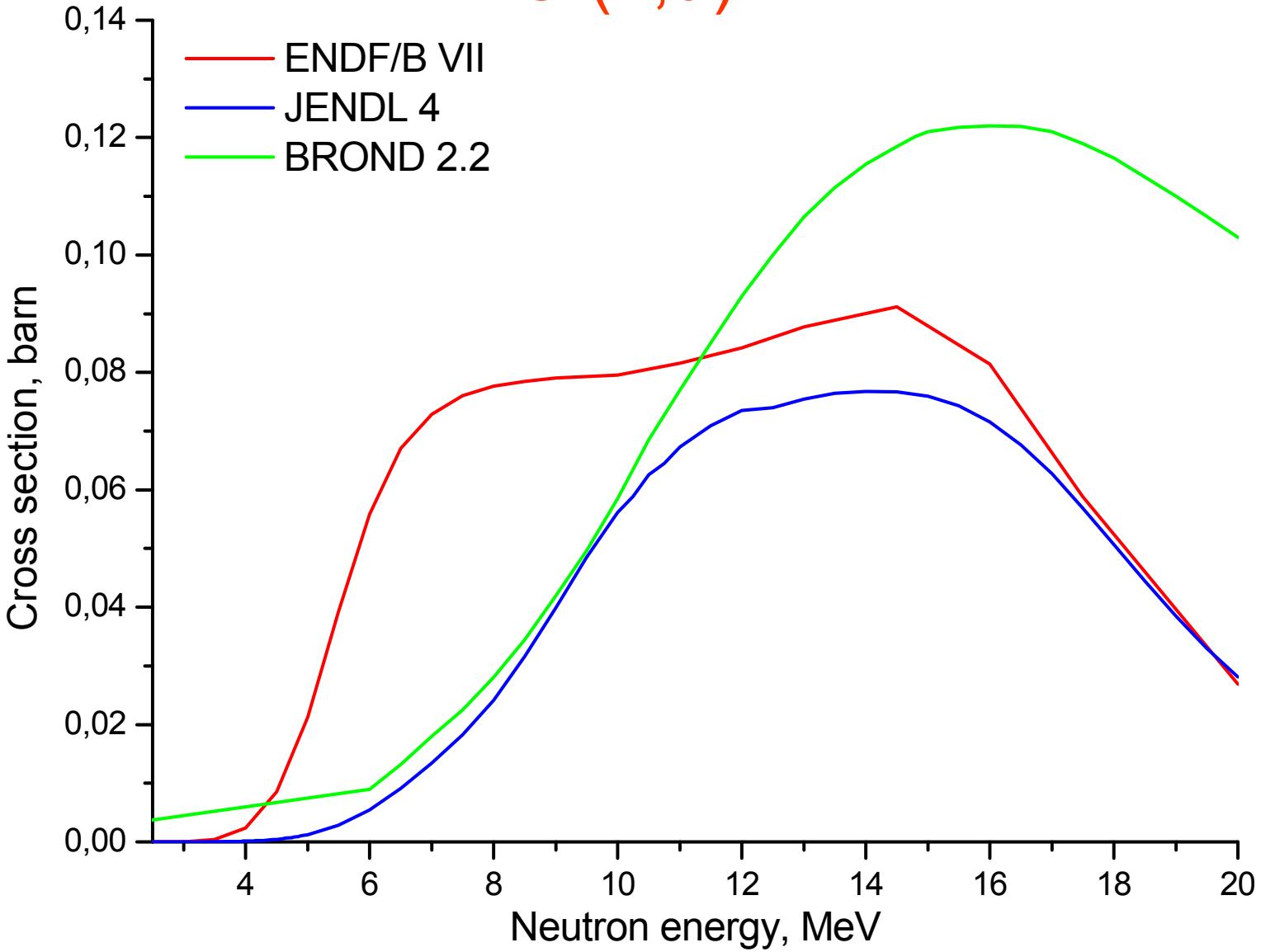

ENDF/B VII to JENDL 3.3 cross section ratio

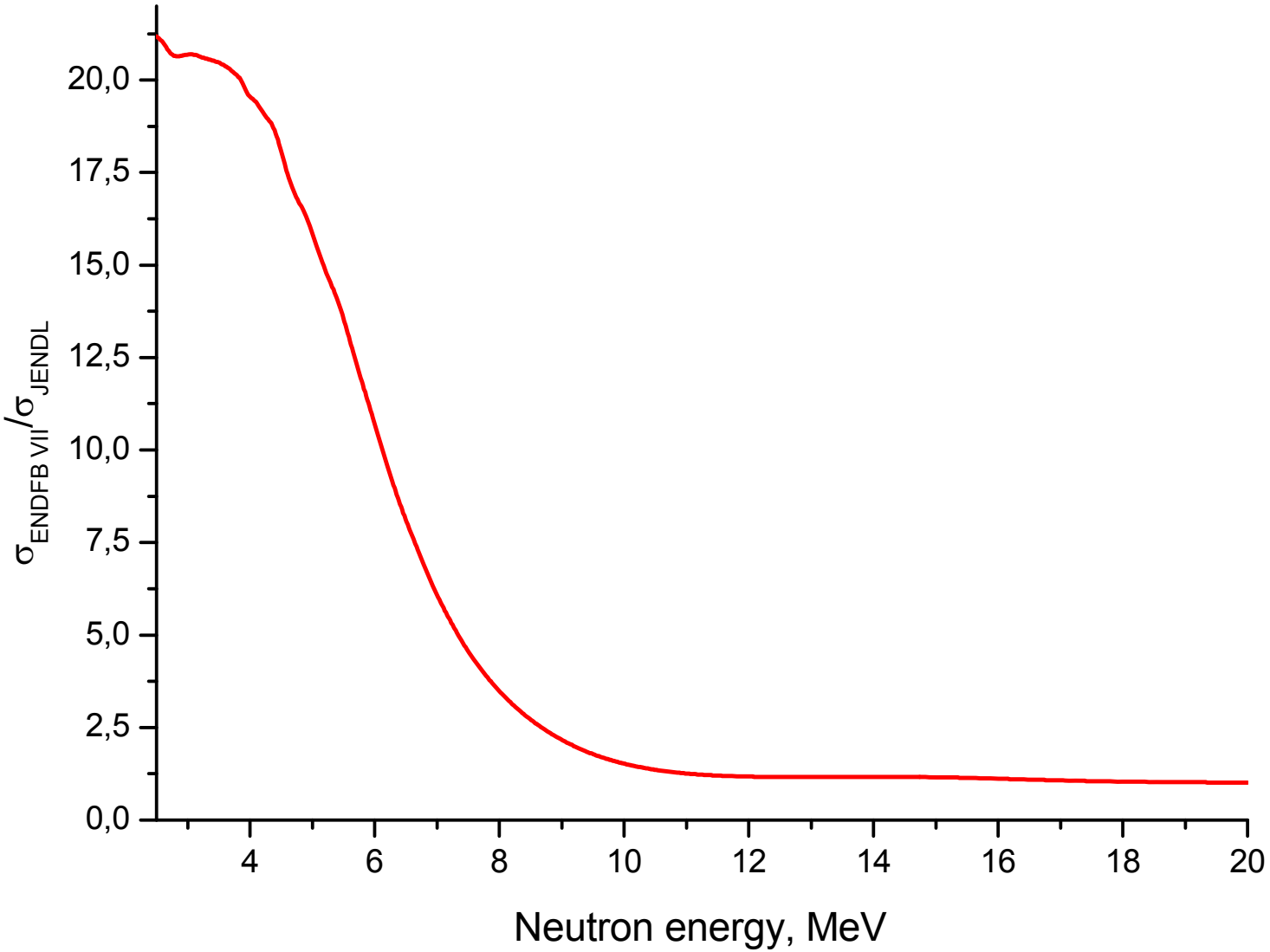

Status of experimental data for $^{50}Cr(n,\alpha)^{47}Ti$ to 2011

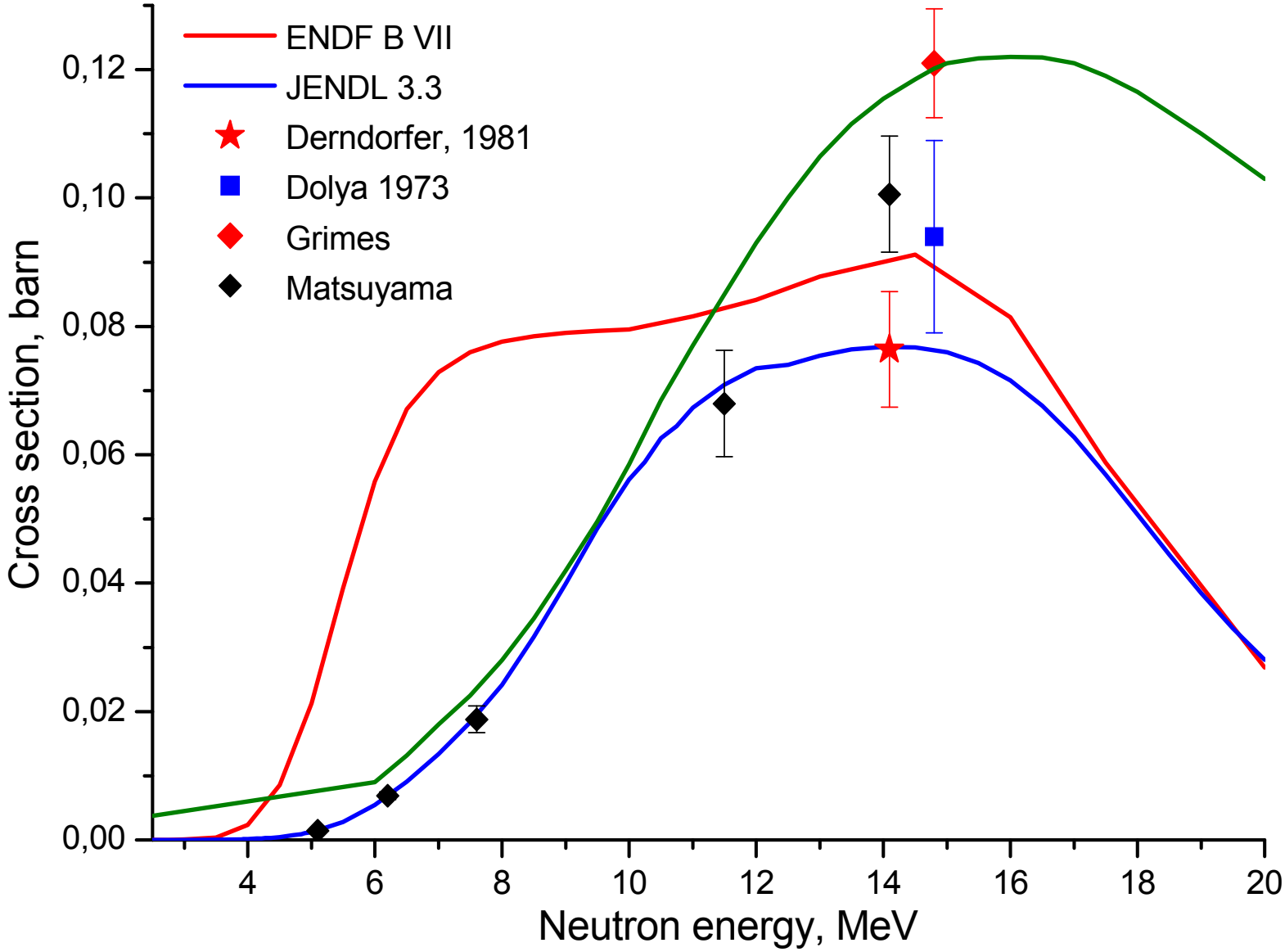

^{50}Cr target parameters

SAMPLE

- **Gold backing of 84 mg/cm^2**
- **^{50}Cr - 365 мкг/см^2**
- **^{50}Cr enriched to 96,8 %**
- **^{52}Cr - 2.98%,**
- **^{53}Cr - 0.18%**
- **^{54}Cr - 0.04%.**

- **Target area – 14,11 cm^2**
- **Total ^{50}Cr mass – 5,15 mg**
- **Total ^{50}Cr number of atoms – 6,22*10^{19}**

C.Derndorfer, R.Fisher, P.Hille, H.Vonach and P.Maier-Komor. Investigation of the ^{50}Cr(n, α)47Ti reaction at En=14.1 MeV. Zeitschrift fur Physic A Hadrons and Nuclei 301, Number 4, pp.327-334

Preliminary result

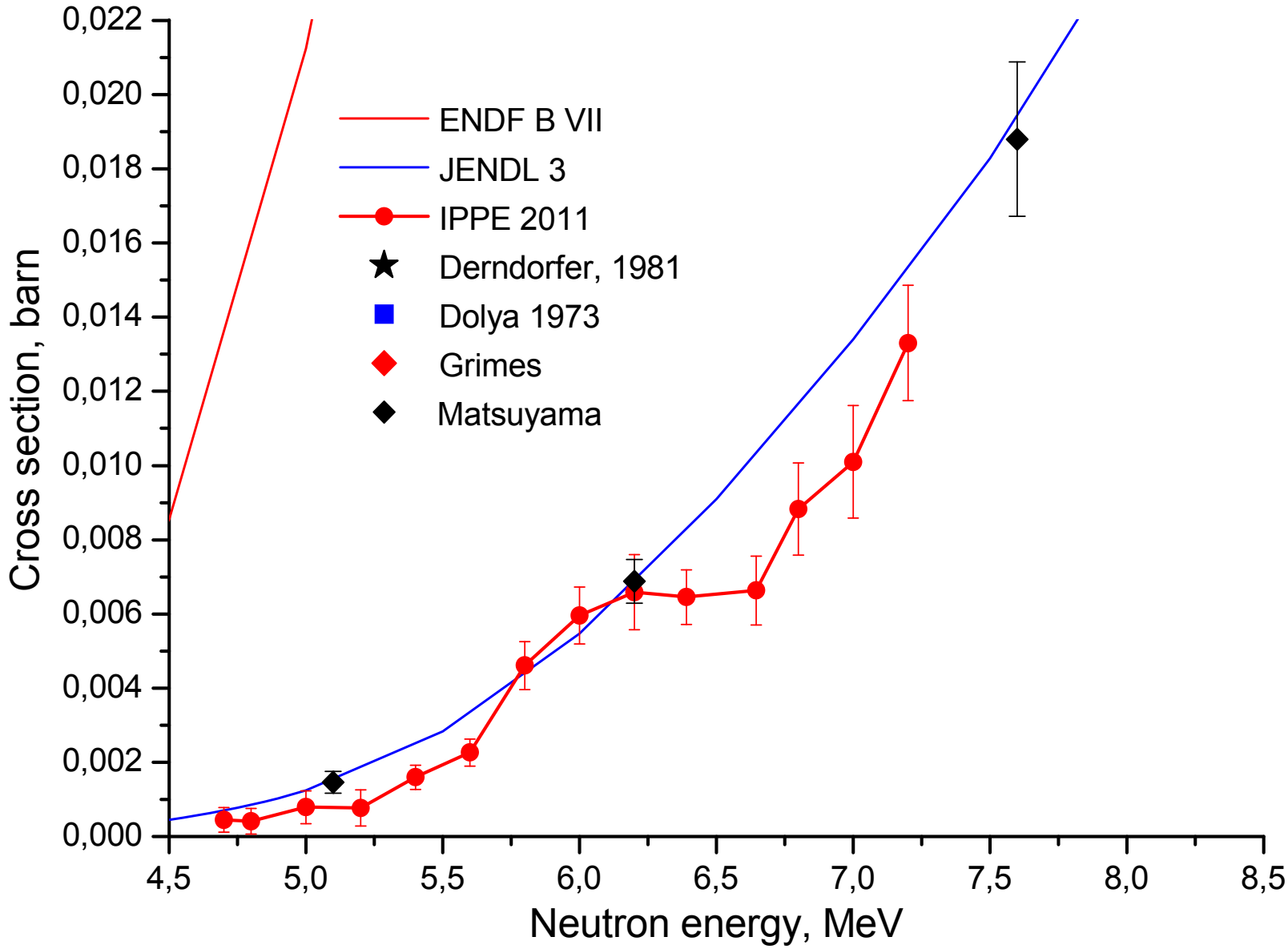

^{52}Cr target

^{52}Cr target on the gold backing - 190 mg/cm^2.
Target diameter – 30.9 mm;
^{52}Cr target was 280 μg/cm^2.
Isotopic composition:
^{50}Cr - 0.1%,
^{52}Cr-99.5%,
^{53}Cr – 0.3%
^{54}Cr – 0.1%.

Total mass of ^{52}Cr is 2.1 mg.

Result for $^{52}Cr(n,\alpha)^{49}Ti$ reaction cross section

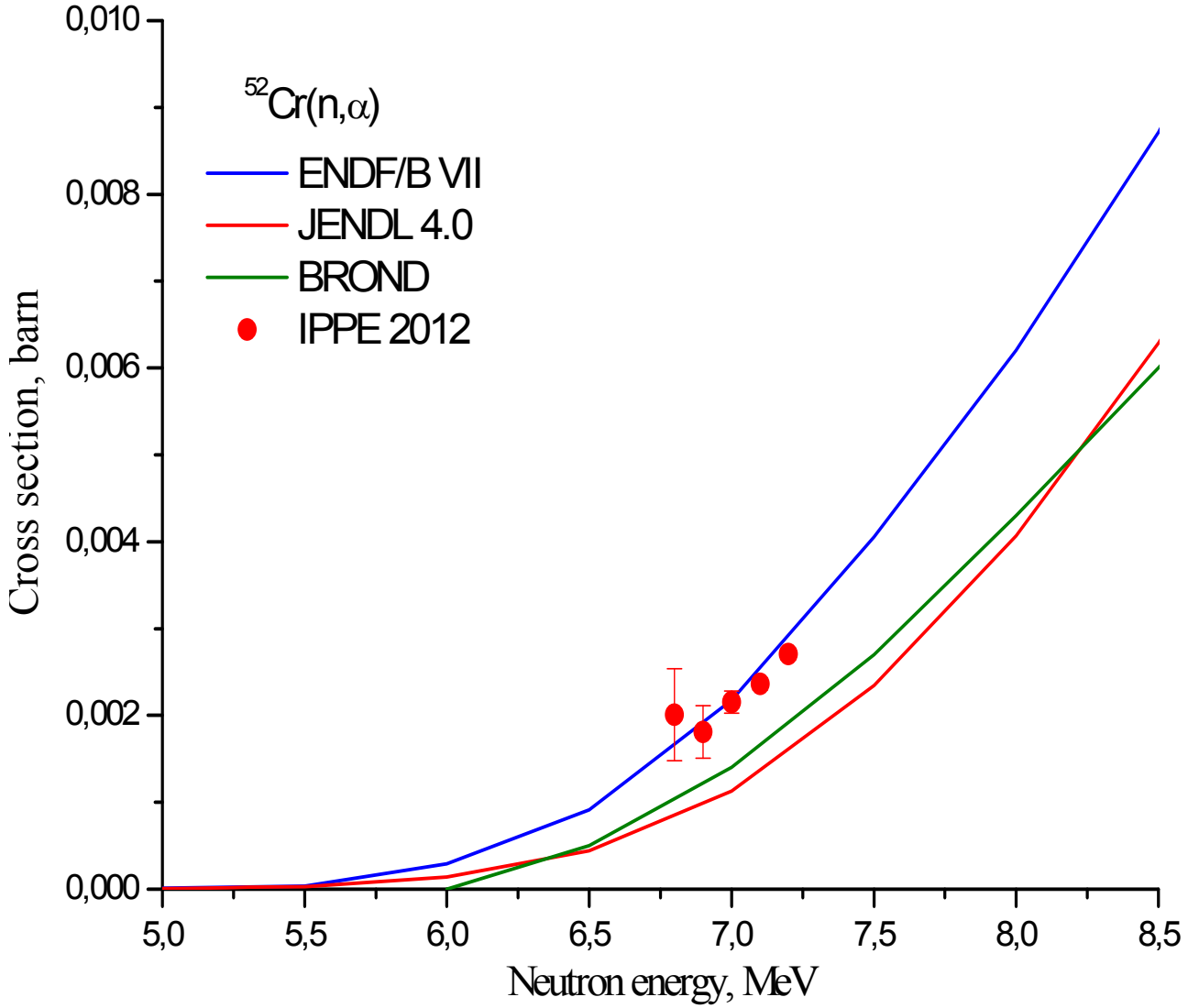

Experimental uncertainties

Counting statistics:

- **Number of the α-particles.**
- **Number of the fission fragments.**

Errors not related to statistics:

- **α-particles "tail" extrapolation – 0,4%.**
- **Fission fragments "tail" extrapolation – 0,6%.**
- **Number of ^{238}U atoms – 1,5%.**
- **^{238}U cross section – 1%.**
- **Number of chromium atoms – 3,2%.**

Total errors not related to statistics – 3,7%.

Typical statistical uncertainty from 2 to 15 %.

Result and plans

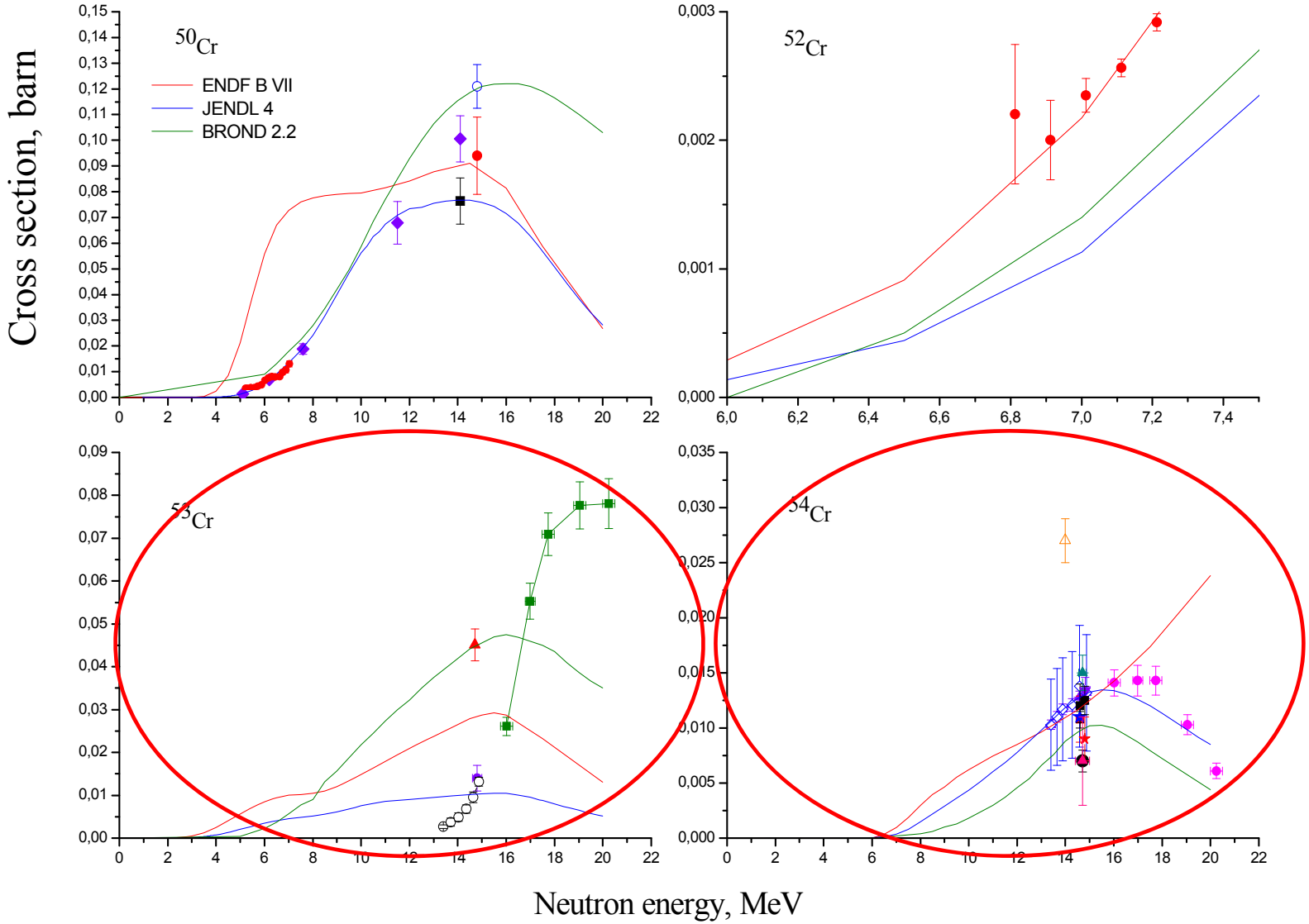

Estimation of (n, alpha) reaction cross section for chromium isotopes

- New digital spectrometer with a solid target for (n, α) reaction cross section investigation was developed.
- Digital algorithms for background suppression was found.
- $^{50}Cr(n,\alpha)^{47}Ti$ cross section in neutron energy region from 4,7 to 7,2 MeV was measured.
- $^{52}Cr(n,\alpha)^{49}Ti$ cross section in neutron energy region from 6,75 to 7,2 MeV was measured.
- Big discrepancy (up to 400%) with ENDF/B VII was found.

DETAILS OF CALCULATIONS

To calculate dose rates, neutron and gamma spectra at different locations in WWER - 440 were obtained using the 3D transport code KATRIN developed by A. Voloschenko et al.

In WWER-1000 the approximate 3D distributions have been received using the 3D synthesis of 2D (*r*,*ϑ*) and (*r*,*z*) and 1D cylindrical (*r*) solutions

PKA-spectra were calculated using the SPECTER code developed by L. Greenwood

TRIGEX code was used for neutron spectra calculations in BN-600.

Data from ENDF/B-VII were used to get displacement cross-sections for considered materials. The processing of the data and the calculation of displacement cross-sections has been performed using the NJOY code, the version 99.161m2.

The displacement cross sections in the energy groups have been averaged over the standard neutron spectrum:

$$F_{cm}(E) = \begin{cases} 1/E & E \le 2.5 \\ e^{-E/0.965} sh\sqrt{2.29E} & E > 2.5 \end{cases}$$

where *E* in MeV.